Article

PD-1 combination therapy with IL-2 modifies CD8$^+$ T cell exhaustion program

https://doi.org/10.1038/s41586-022-05257-0

Received: 15 March 2021

Accepted: 22 August 2022

Published online: 28 September 2022

Check for updates

Masao Hashimoto[1,2], Koichi Araki[1,2,3,4], Maria A. Cardenas[5], Peng Li[6], Rohit R. Jadhav[7,8], Haydn T. Kissick[1,2,5,9], William H. Hudson[1,2], Donald J. McGuire[1,2], Rebecca C. Obeng[1,2,10,11], Andreas Wieland[1,2,12,13], Judong Lee[1,2], Daniel T. McManus[1,2], James L. Ross[1,2], Se Jin Im[1,2,14], Junghwa Lee[1,2,15], Jian-Xin Lin[6], Bin Hu[8], Erin E. West[6,16], Christopher D. Scharer[2], Gordon J. Freeman[17,18], Arlene H. Sharpe[19,20], Suresh S. Ramalingam[9,21], Alex Pellerin[22], Volker Teichgräber[23], William J. Greenleaf[24], Christian Klein[25], Jorg J. Goronzy[7,8], Pablo Umaña[25], Warren J. Leonard[6], Kendall A. Smith[26] & Rafi Ahmed[1,2,9] ✉

Combination therapy with PD-1 blockade and IL-2 is highly effective during chronic lymphocytic choriomeningitis virus infection[1]. Here we examine the underlying basis for this synergy. We show that PD-1 + IL-2 combination therapy, in contrast to PD-1 monotherapy, substantially changes the differentiation program of the PD-1$^+$TCF1$^+$ stem-like CD8$^+$ T cells and results in the generation of transcriptionally and epigenetically distinct effector CD8$^+$ T cells that resemble highly functional effector CD8$^+$ T cells seen after an acute viral infection. The generation of these qualitatively superior CD8$^+$ T cells that mediate viral control underlies the synergy between PD-1 and IL-2. Our results show that the PD-1$^+$TCF1$^+$ stem-like CD8$^+$ T cells, also referred to as precursors of exhausted CD8$^+$ T cells, are not fate-locked into the exhaustion program and their differentiation trajectory can be changed by IL-2 signals. These virus-specific effector CD8$^+$ T cells emerging from the stem-like CD8$^+$ T cells after combination therapy expressed increased levels of the high-affinity IL-2 trimeric (CD25–CD122–CD132) receptor. This was not seen after PD-1 blockade alone. Finally, we show that CD25 engagement with IL-2 has an important role in the observed synergy between IL-2 cytokine and PD-1 blockade. Either blocking CD25 with an antibody or using a mutated version of IL-2 that does not bind to CD25 but still binds to CD122 and CD132 almost completely abrogated the synergistic effects observed after PD-1 + IL-2 combination therapy. There is considerable interest in PD-1 + IL-2 combination therapy for patients with cancer[2,3], and our fundamental studies defining the underlying mechanisms of how IL-2 synergizes with PD-1 blockade should inform these human translational studies.

The PD-1 inhibitory pathway has a central role in regulating T cell exhaustion during chronic viral infection and cancer, and PD-1-directed immunotherapy is approved for the treatment of several different cancers[4,5]. However, not all patients respond to PD-1 monotherapy and there is considerable interest in developing PD-1 combination therapies to improve the overall response rate and also get more complete and durable responses in patients with cancer. Many different combination-therapy approaches are currently being tested in animal models and also in clinical trials. One potentially promising candidate for combination therapy with PD-1 blockade is the common γ-chain cytokine interleukin-2 (IL-2)[2,3,6]. The rationale here is to remove the PD-1 inhibitory brake and, at the same time, provide a positive signal

[1]Emory Vaccine Center, Emory University School of Medicine, Atlanta, GA, USA. [2]Department of Microbiology and Immunology, Emory University School of Medicine, Atlanta, GA, USA. [3]Division of Infectious Diseases, Center for Inflammation and Tolerance, Cincinnati Children's Hospital Medical Center, Cincinnati, OH, USA. [4]Department of Pediatrics, University of Cincinnati College of Medicine, Cincinnati, OH, USA. [5]Department of Urology, Emory University School of Medicine, Atlanta, GA, USA. [6]Laboratory of Molecular Immunology and the Immunology Center, National Heart, Lung, and Blood Institute (NHLBI), National Institutes of Health (NIH), Bethesda, MD, USA. [7]Department of Immunology, Mayo Clinic School of Medicine and Sciences, Rochester, MN, USA. [8]Department of Medicine, Division of Immunology and Rheumatology, Stanford University School of Medicine, Stanford, CA, USA. [9]Winship Cancer Institute, Emory University, Atlanta, GA, USA. [10]Department of Pathology, Emory University School of Medicine, Atlanta, GA, USA. [11]Department of Pathology and Robert H. Lurie Comprehensive Cancer Center, Northwestern University Feinberg School of Medicine, Chicago, IL, USA. [12]Department of Otolaryngology, The Ohio State University College of Medicine, Columbus, OH, USA. [13]The Pelotonia Institute for Immuno-Oncology, The Ohio State University Comprehensive Cancer Center, Columbus, OH, USA. [14]Department of Immunology, Sungkyunkwan University School of Medicine, Suwon, Republic of Korea. [15]Department of Precision Medicine, Sungkyunkwan University School of Medicine, Suwon, Republic of Korea. [16]Complement and Inflammation Research Section (CIRS), National Heart, Lung, and Blood Institute (NHLBI), National Institutes of Health (NIH), Bethesda, MD, USA. [17]Department of Medical Oncology, Dana-Farber Cancer Institute, Boston, MA, USA. [18]Department of Medicine, Harvard Medical School, Boston, MA, USA. [19]Department of Immunology, Blavatnik Institute, Harvard Medical School, Boston, MA, USA. [20]Evergrande Center for Immunological Diseases, Harvard Medical School and Brigham and Women's Hospital, Boston, MA, USA. [21]Department of Hematology and Medical Oncology, Emory University School of Medicine, Atlanta, GA, USA. [22]Biogen, Cambridge, MA, USA. [23]Roche Innovation Center Basel, Basel, Switzerland. [24]Department of Genetics, Stanford University School of Medicine, Stanford, CA, USA. [25]Roche Innovation Center Zurich, Schlieren, Switzerland. [26]Department of Medicine, Division of Immunology, Weill Medical College of Cornell University, New York, NY, USA. ✉e-mail: rahmed@emory.edu

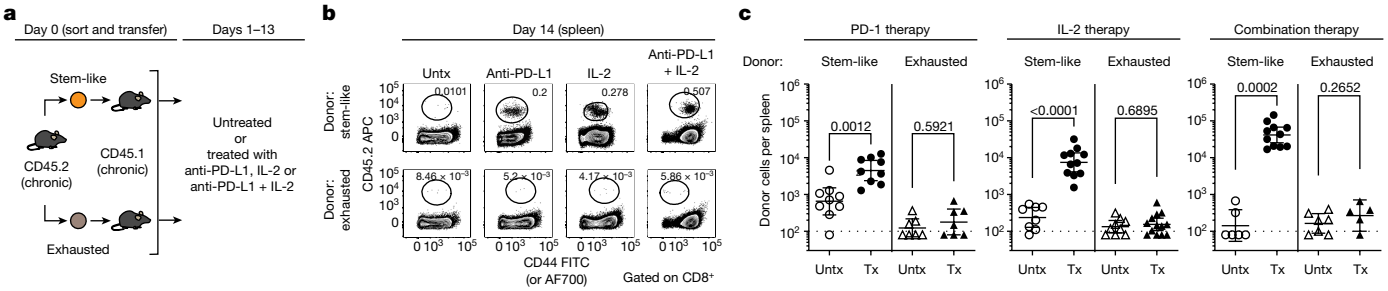

Fig. 1 | PD-1$^+$TCF1$^+$ stem-like CD8$^+$ T cells provide the proliferative burst after PD-1 blockade, IL-2 therapy and PD-1 + IL-2 combination therapy during chronic LCMV infection. a, The stem-like (PD-1$^+$CXCR5$^+$TIM3$^-$) and terminally differentiated exhausted (PD-1$^+$CXCR5$^-$TIM3$^+$) CD8$^+$ T cell subsets were sorted from the spleens of LCMV chronically infected CD45.2$^+$ mice and each subset was transferred into infection-matched CD45.1$^+$ recipient mice. Groups of these mice were then either left untreated, or given anti-PD-L1 antibodies, IL-2 therapy or the PD-1 + IL-2 combination therapy for 2 weeks. **b**, Representative FACS analysis of the frequency of donor CD45.2$^+$CD8$^+$ T cells in the recipient mice 2 weeks after the various treatments. **c**, The numbers of donor CD45.2$^+$CD8$^+$ T cells after 2 weeks of the indicated treatments. Results were pooled from 3 or 4 experiments with $n = 7–9$ (PD-1 therapy), $n = 8–13$ (IL-2 therapy) and $n = 5–11$ (combination therapy) per group. Data are geometric mean ± 95% confidence interval (CI). The dotted lines indicate the limit of detection of donor CD45.2$^+$CD8$^+$ T cells. *P* values are shown; statistical comparisons were performed using two-tailed unpaired Mann–Whitney *U*-tests. AF, Alexa Fluor; Tx, treated; Untx, untreated.

for T cells with IL-2—a cytokine that was originally defined as a growth factor for T cells[7]. There are currently several clinical trials of PD-1 + IL-2 combination therapy that are ongoing for cancer[2,3]. Thus, it is important to better understand how this combination therapy works and to define the cellular and molecular bases for the observed synergy between PD-1 blockade and IL-2.

Viral control by CD8$^+$ T cells after PD-1 + IL-2 therapy

The mouse model of chronic lymphocytic choriomeningitis virus (LCMV) infection was used to examine the synergy between PD-1 blockade and IL-2 cytokine therapy. Groups of chronically infected mice were either left untreated, treated with anti-PD-L1 antibodies alone, given IL-2 alone, or given combination therapy with anti-PD-L1 antibodies and IL-2. Combination therapy resulted in highly synergistic increases in the number of functional LCMV-specific CD8$^+$ T cells and significantly better viral control in both lymphoid and non-lymphoid tissues (Extended Data Fig. 1a–e). These results are consistent with our earlier observations[1]. We next determined whether this enhanced viral control after PD-1 + IL-2 combination therapy was mediated by CD8$^+$ T cells by treating mice with anti-CD8 depleting antibodies during the period of combination therapy. Depletion of CD8$^+$ T cells almost completely abrogated the antiviral effect observed after PD-1 + IL-2 combination treatment. There was a strong correlation between the number of CD8$^+$ T cells (total and LCMV-specific) and reduction in the viral titre in the spleen, liver and lungs of these mice (Extended Data Fig. 1f–i). Thus, viral control after PD-1 + IL-2 combination therapy is mediated by LCMV-specific CD8$^+$ T cells.

PD-1$^+$TCF1$^+$CD8$^+$ T cells respond to PD-1 + IL-2 therapy

Recent studies have identified a population of PD-1$^+$TCF1$^+$ stem-like CD8$^+$ T cells that function as a resource cell for maintaining the CD8$^+$ T cell response during chronic viral infection and cancer and also provide the proliferative burst after PD-1 blockade[8–14]. A key was whether these PD-1$^+$ stem-like CD8$^+$ T cells also respond to PD-1 + IL-2 combination therapy. To address this question, we sorted the PD-1$^+$ stem-like CD8$^+$ T cells or the more differentiated/exhausted cell population from LCMV chronically infected mice using appropriate cell-surface markers and transferred these cells into infection-matched mice. Groups of these mice were then treated with PD-1 blockade alone, IL-2 alone, or both PD-1 blockade and IL-2 (Fig. 1a and Extended Data Fig. 2a). These T cell adoptive transfer experiments were performed using congenically distinct mice so that donor and recipient CD8$^+$ T cells could be easily distinguished. We found that the response to PD-1 blockade came exclusively from the stem-like CD8$^+$ T cells, confirming our earlier studies[8,10,13]. Interestingly, the response to IL-2 therapy alone and to PD-1 + IL-2 combination therapy also came from the PD-1$^+$ stem-like CD8$^+$ T cells. By contrast, there was minimal to no response from the more differentiated CD8$^+$ T cell population after any of these three treatments. Notably, the magnitude of the response from the stem-like CD8$^+$ T cells was about tenfold greater after combination therapy compared with after PD-1 monotherapy. This was seen in multiple tissues, including the spleen, liver, lungs and blood (Fig. 1b,c and Extended Data Fig. 2b–d). Taken together, these results show that the same population of PD-1$^+$TCF1$^+$CD8$^+$ T cells responds to PD-1 blockade, IL-2 treatment and PD-1 + IL-2 combination therapy, highlighting the importance of these CD8$^+$ T cells in different immunotherapy regimens.

Transcriptional signature of LCMV-specific CD8$^+$ T cells

The studies above showed that the same precursor stem-like CD8$^+$ T cells responded by proliferation and differentiation to all of the treatments. Thus, it was of interest to determine whether the transcriptional signatures of the expanded CD8$^+$ T cells were similar or different after PD-1 monotherapy versus combination therapy or IL-2 treatment alone. RNA-sequencing (RNA-seq) analysis was performed in sorted LCMV-specific CD8$^+$ T cells (D^{b}GP33$^+$) from the four groups of chronically infected mice. The RNA-seq results showed that the gene expression profile of virus-specific CD8$^+$ T cells was similar in untreated mice compared to mice treated with PD-1 blockade alone. However, PD-1 + IL-2 combination therapy resulted in LCMV-specific CD8$^+$ T cells with a transcriptional signature that was notably different from what was observed after PD-1 monotherapy. Interestingly, IL-2 treatment alone also gave LCMV-specific CD8$^+$ T cells with a gene expression profile similar to the combination therapy (Fig. 2a,b and Extended Data Fig. 3a). Expression of several inhibitory receptors (*Havcr2*, *Pdcd1*, *Lag3*, *Tigit*, *Cd101*, *Cd160*, *Cd244* and *Btla*) and transcription factors associated with T cell exhaustion (*Batf*, *Egr2*, *Ikzf2*, *Irf4*, *Nfatc1*, *Nr4a2* and *Tox2*)[4,5,9,15,16] were downregulated in LCMV-specific CD8$^+$ T cells from mice that received PD-1 + IL-2 combination therapy or IL-2 treatment alone compared with virus-specific CD8$^+$ T cells isolated from untreated chronically infected mice or after PD-1 monotherapy. Interestingly, in contrast to the downregulation of genes associated with exhaustion, there was upregulation of genes encoding effector molecules and inflammatory cytokine receptors (*Gzmb*, *Il18r1*, *Il18rap* and *Il1rl1* (also known as ST2, a receptor for IL-33)) in mice receiving combination therapy or IL-2 treatment. There was also increased RNA

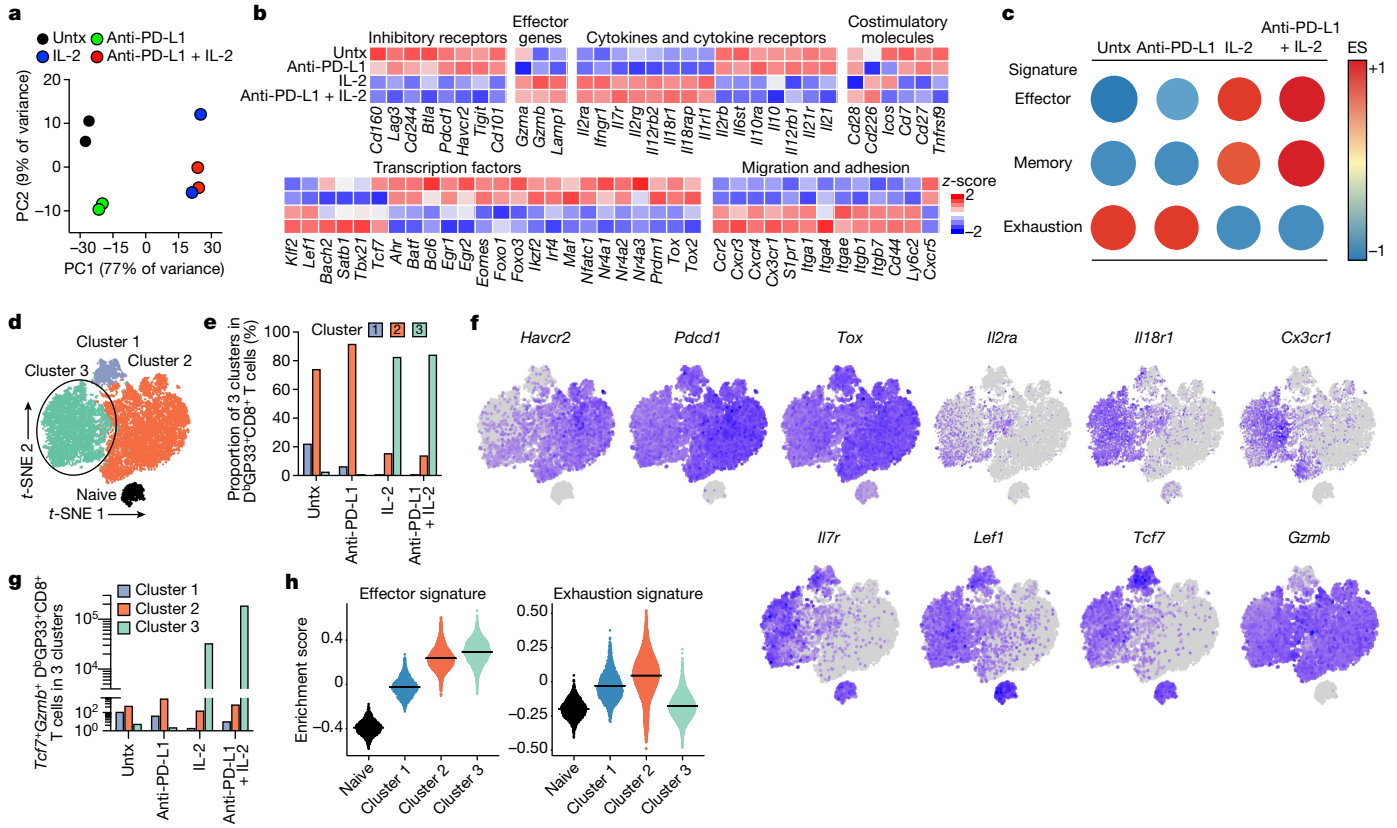

Fig. 2 | Distinct transcriptional signature of virus-specific CD8$^+$ T cells after PD-1 + IL-2 combination therapy compared to PD-1 monotherapy during chronic LCMV infection. a–**h**, Mice chronically infected with LCMV were treated with PD-1 monotherapy, IL-2 alone or PD-1 + IL-2 combination therapy for 2 weeks. LCMV-specific D^{b}GP33$^+$CD8$^+$ T cells from spleens of each treatment group were sorted for RNA-seq (**a**–**c**) and scRNA-seq (**d**–**h**) analysis. As a control, naive CD44^{low}CD8$^+$ T cells were also sorted for scRNA-seq (**d**–**h**). **a**, PCA plot of D^{b}GP33$^+$CD8$^+$ T cells after the indicated treatments. **b**, The mean relative expression of specific genes. **c**, GSEA of D^{b}GP33$^+$CD8$^+$ T cells generated by the indicated treatments for the effector and memory signatures (acute infection) and the exhaustion signature (chronic infection). The colour and size of the circles represent the enrichment score (ES) for each signature. **d**, *t*-SNE projections of naive CD44^{low}CD8$^+$ T cells and D^{b}GP33$^+$CD8$^+$ T cells generated by the various treatments. Four clusters (one for naive and three for treatment samples) were defined and are indicated by different colours. The new cluster (cluster 3) generated after combination therapy or IL-2 treatment is highlighted by the black circle. **e**, The proportions of three clusters in D^{b}GP33$^+$CD8$^+$ T cells in each treatment group. **f**, Normalized expression of several representative genes is shown within the four clusters. **g**, The numbers of *Tcf7*$^+$*Gzmb*$^+$ D^{b}GP33$^+$CD8$^+$ T cells that are present in clusters 1, 2 and 3 after the various treatments. **h**, GSEA of D^{b}GP33$^+$CD8$^+$ T cells in each of three clusters for effector signature (acute infection) and exhaustion signature (chronic infection). The enrichment score for the signature in each cluster is shown as violin plots; the horizontal bars show the mean. Results were pooled from 2 (**a**–**c**) and 1 or 2 (**d**–**h**) experiments with $n = 2$–18 mice per group in each experiment.

levels for some memory-associated genes (*Il7r* and *Lef1*)[16]. One of the most notable changes in LCMV-specific CD8$^+$ T cells after combination or IL-2 therapy was the upregulation of genes involved in migration and adhesion (*Cxcr3*, *S1pr1*, *Klf2*, *Itgb1*, *Cd44* and *Ly6c2*). These transcriptional changes are consistent with PD-1 + IL-2 combination therapy resulting in the generation of LCMV-specific CD8$^+$ T cells that resemble CD8$^+$ effector (T_{eff}) and memory (T_{mem}) T cells generated during acute infection rather than exhausted CD8$^+$ T cells present during chronic infection[9,16,17]. To further confirm these observations, gene set enrichment analysis (GSEA) was performed using signatures of CD8$^+$ T cell exhaustion from LCMV clone 13 chronic infection and CD8$^+$ T cell effector and memory signatures from LCMV Armstrong acute infection[16,17]. The GSEA results show that LCMV-specific CD8$^+$ T cells from the combination therapy or IL-2 treatment showed a decrease in the exhaustion signature and an enrichment for the acute effector and memory signatures. The opposite pattern was seen with virus-specific CD8$^+$ T cells from untreated chronically infected mice or after PD-1 monotherapy (Fig. 2c and Extended Data Fig. 3b–d).

To gain further insights into how the differentiation program of virus-specific CD8$^+$ T cells was altered by PD-1 + IL-2 combination therapy versus PD-1 monotherapy, we performed single-cell RNA sequencing (scRNA-seq) analysis of LCMV-specific CD8$^+$ T cells after the various in vivo treatments. We compared these different tetramer-sorted cells along with naive CD8$^+$ T cells using *t*-distributed stochastic neighbour embedding (*t*-SNE) projection analysis. This analysis displayed four clusters, one for naive CD8$^+$ T cells (naive cluster) and the other three for the LCMV-specific CD8$^+$ T cell samples (clusters 1–3) (Fig. 2d). We found that D^{b}GP33-specific CD8$^+$ T cells from untreated and PD-1-treated mice were mostly composed of cluster 1 and 2, which represented clusters for PD-1$^+$TCF1$^+$ stem-like cells (cluster 1) and the more differentiated CD8$^+$ T cells (cluster 2). By contrast, LCMV-specific CD8$^+$ T cells from mice treated with IL-2 alone or given the combination therapy consisted predominantly (>80%) of the unique cluster 3. Note that PD-1 + IL-2 combination therapy reduces the percentage of cells in cluster 1 but there is no decrease in the total numbers of the stem-like CD8$^+$ T cells (Fig. 2e and Extended Data Fig. 3e–g). The dominance of cluster 3 is quite striking and it is this cluster that defines the new LCMV-specific CD8$^+$ T cell population that is generated from the PD-1$^+$TCF1$^+$ stem-like CD8$^+$ T cells after treatment of chronically infected mice with IL-2 or combination therapy. This cluster is characterized by lower expression of multiple inhibitory receptors and transcription factors that are associated with T cell exhaustion and upregulation of genes

related to effector function, migration and adhesion. Cluster 3 cells also expressed some genes associated with T_{mem} cells (*Tcf7*, *Lef1* and *Il7r*) (Fig. 2f and Extended Data Fig. 3h). We were particularly interested in whether there were any virus-specific $CD8^+$ T cells that co-express *Tcf7* and *Gzmb*. Cluster 1, which represents the PD-1^+ stem-like $CD8^+$ T cells, consisted mostly (90%) of *Tcf7*$^+$ cells that did not express *Gzmb* and cluster 2, which represents the more differentiated population, comprised mostly (96%) *Gzmb*-positive cells that did not express *Tcf7*. By contrast, more than 20% of $CD8^+$ T cells in the unique cluster 3 co-expressed *Tcf7* and *Gzmb* resulting in more than 10^5 LCMV-specific $CD8^+$ T cells in the spleen co-expressing *Tcf7* and *Gzmb* after combination therapy and 3×10^4 cells after IL-2 therapy compared to <500–4,000 such cells in mice that were untreated or given PD-1 monotherapy (Fig. 2g and Extended Data Fig. 3i). These $CD8^+$ T cells are of biological importance because memory precursor effector $CD8^+$ T cells that are generated during acute infections and give rise to the pool of long-lived $CD8^+$ T_{mem} cells also co-express *Gzmb* and *Tcf7*[18–20]. GSEA of the three clusters showed that cluster 3 cells were enriched for the effector signature and the exhaustion signature was highly decreased in contrast to in cluster 2 cells generated after PD-1 monotherapy that were enriched for effector signature but were also highly enriched for the exhaustion signature (Fig. 2h). A similar pattern was seen when GSEA was performed using the different treatment groups as opposed to the different clusters (Extended Data Fig. 3j).

Phenotype and function of LCMV-specific $CD8^+$ T cells

To determine whether the key changes in the transcriptional signatures were also reflected by protein expression, we performed extensive fluorescence-activated cell sorting (FACS) analysis of LCMV-specific $CD8^+$ T cells isolated from chronically infected mice that were untreated, given PD-1 therapy, IL-2 treatment or combination therapy. These phenotypic analyses are shown in Extended Data Fig. 4a and they confirm the RNA-seq data. The phenotypic markers expressed by LCMV-specific $CD8^+$ T cells after combination therapy or IL-2 treatment are consistent with these $CD8^+$ T cells being less exhausted and more effector-like plus expressing some T_{mem} cell markers. We also performed multiparameter flow cytometry, and this confirmed the scRNA-seq data showing that the expanded $CD8^+$ T cells after IL-2 treatment or PD-1 + IL-2 combination therapy were dominated by a unique cluster 3 that comprised around 90% of the cell population. The virus-specific $CD8^+$ T cells in cluster 3 express effector molecules such as granzyme B, CX3CR1 and CD218a but, at the same time, also express markers associated with stem-like $CD8^+$ T cells such as TCF1, SLAMF6 and CD73. These $CD8^+$ T cells also express lower levels of exhaustion markers such as TIM3 and CD101 (Fig. 3a–c and Extended Data Fig. 5a).

The virus-specific $CD8^+$ T cells generated after PD-1 + IL-2 combination therapy were also functionally superior to $CD8^+$ T cells generated after PD-1 monotherapy. As shown in Extended Data Fig. 1c,d, these $CD8^+$ T cells produced multiple cytokines and degranulated after peptide stimulation, and this cytokine production comes predominantly from the unique cluster 3 $CD8^+$ T cells generated after the combination therapy (Fig. 3d and Extended Data Fig. 5b). In addition to efficient cytokine production after stimulation with virus-specific peptides, the LCMV-specific $CD8^+$ T cells generated after PD-1 + IL-2 combination therapy or IL-2 treatment could also produce IFNγ after stimulation by IL-12 and IL-18 in the absence of peptide stimulation. This is due to the high expression of IL-18Rα (also known as CD218a) by these $CD8^+$ T cells. An interesting biological consequence of CD218a expression is that these $CD8^+$ T cells can respond to inflammatory cytokines (IL-12 and IL-18) and produce IFNγ even in the absence of cognate antigen (Extended Data Fig. 4b,c). Similar to the cytokine production seen after stimulation with LCMV-specific peptides, the IL-12- and IL-18-mediated release of IFNγ in the absence of antigen stimulation also comes from cluster 3 $CD8^+$ T cells generated after PD-1 + IL-2 combination therapy (Fig. 3e). Another interesting biological property of the LCMV-specific $CD8^+$ T cells generated after combination therapy or IL-2 treatment is their ability to migrate to CXCL9 and CXCL10 due to the high expression of the chemokine receptor CXCR3 (Fig. 3c,f and Extended Data Fig. 4a). CXCR3 has an important role in $CD8^+$ T cell mediated viral control and a role for CXCL9 and CXCL10 has been implicated in cancer immunotherapy[21,22].

Epigenetic signature of LCMV-specific $CD8^+$ T cells

Virus-specific $CD8^+$ T cells acquire an epigenetic landscape during chronic infection that is distinct from that of $CD8^+$ T_{eff} and T_{mem} cells during acute infection, and the epigenetic stability of this exhaustion program has been proposed to limit the effectiveness of PD-1 therapy[23,24]. We next examined whether PD-1 + IL-2 combination therapy changed the epigenetic signatures of LCMV-specific $CD8^+$ T cells using the assay for transposase-accessible chromatin with sequencing (ATAC-seq)[25]. PD-1 + IL-2 combination therapy substantially changed the chromatin accessibility of LCMV-specific $CD8^+$ T cells compared with virus-specific $CD8^+$ T cells from untreated mice or mice treated with PD-1 monotherapy (Fig. 4a). IL-2 treatment alone also induced changes in the epigenetic signature of LCMV-specific $CD8^+$ T cells compared with untreated mice (Fig. 4a). The differentially open and closed regions after PD-1 + IL-2 combination therapy versus PD-1 monotherapy were identified using the Genomic Regions Enrichment of Annotations Tool (GREAT)[26] and Gene Ontology (GO) analysis. Pathways related to cytokine and chemokine receptor activity, S1P signalling and lymphocyte trafficking were highly enriched after combination therapy (Supplementary Data 1 and 2). Examples of several immunologically relevant genes that are more open in virus-specific $CD8^+$ T cells after PD-1 + IL-2 combination therapy compared with after PD-1 therapy are shown in Fig. 4b and Extended Data Fig. 6a. Genes involved in chemokine and cytokine responses, effector functions and transcription factors such as *Tcf7*, *Lef1*, *Klf2* and *Tbx21* were more accessible after combination therapy, whereas genes for inhibitory receptors and *Tox*—an important regulator of T cell exhaustion[15,27–29]—were more open after PD-1 monotherapy (Fig. 4b and Extended Data Fig. 6a,b).

We next compared the epigenetic signatures of the virus-specific $CD8^+$ T cells from these various treated samples with the epigenetic signatures of the $CD8^+$ T_{eff} cell subsets—memory precursor and terminal effector—and T_{mem} cells from acute infection[30]. Principal component analysis (PCA) analysis of the 5,000 most variable sites showed that the epigenetic signatures of LCMV-specific $CD8^+$ T cells after PD-1 + IL-2 combination therapy or IL-2 monotherapy were more similar to $CD8^+$ T_{eff} and T_{mem} cells after acute infection compared with virus-specific $CD8^+$ T cells after PD-1 monotherapy or from untreated chronically infected mice (Fig. 4c). *k*-Means clustering of the sites that changed with treatment revealed that ten clusters were formed, as shown in the heat plot for all of the different $CD8^+$ T cell subsets (Extended Data Fig. 6c). Clusters showing patterns resembling acute infection by sites opening in the IL-2 treatment or the combination treatment (clusters 2–4) groups had increased accessibility to transcription factors of the zinc-finger, runt and T-box families, whereas sites closing (clusters 5–7) after IL-2 or combination therapy showed enrichment for transcription factors of the bZIP, RHD (NFAT) and NR (Nur77) families (Extended Data Fig. 6c and Supplementary Data 3). Of particular interest is the closing of RHD sites after IL-2 treatment or PD-1 + IL-2 combination therapy because NFAT has been implicated in inducing exhaustion and the upregulation of Tox expression[15,27–29]. Accordingly, multiple regulatory regions of the *Tox* gene were highly accessible in untreated cells or cells treated with PD-1, but no longer accessible in IL-2 or the combination therapy samples. Taken together, these results demonstrate that the epigenetic program of virus-specific $CD8^+$ T cells during chronic infection can be modified by PD-1 + IL-2 combination therapy resulting in cells that resemble more functional $CD8^+$ T_{eff} and T_{mem} cells generated

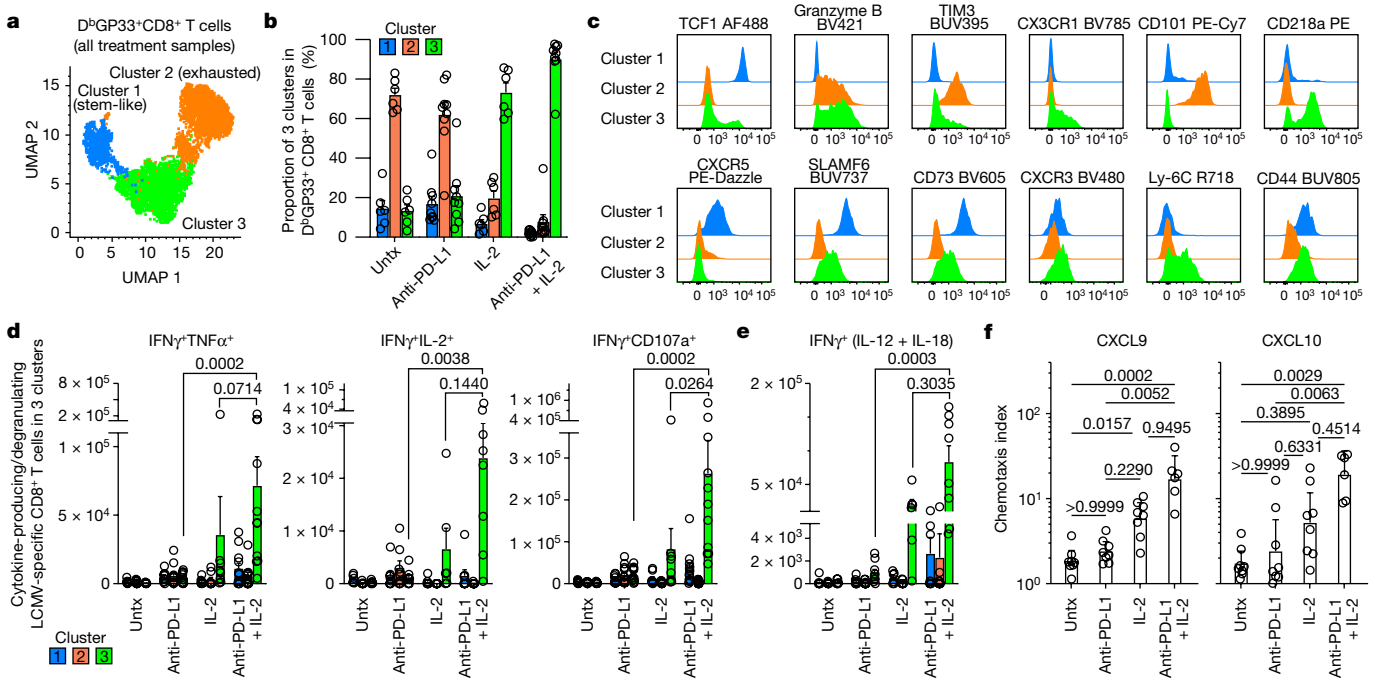

Fig. 3 | Phenotypic and functional characterization of LCMV-specific CD8⁺ T cells generated by PD-1 and IL-2 monotherapy and the combination therapy during chronic infection. LCMV chronically infected mice were either untreated or treated with PD-1 therapy, IL-2 treatment or the PD-1 + IL-2 combination therapy for 2 weeks. **a**, Representative UMAP analysis with FlowSOM overlay showing three clusters of concatenated $D^bGP33^+CD8^+$ T cells isolated from spleens after the four treatments. **b**, The proportions of three clusters of $D^bGP33^+CD8^+$ T cells in the different groups of mice. **c**, Representative histograms of various phenotypic markers expressed by $D^bGP33^+CD8^+$ T cells in the three clusters. **d**, Effector function in response to stimulation with LCMV-specific peptides. Spleen cells were stimulated with pools of LCMV-specific peptides for 5 h and analysed by intracellular staining for cytokine production and degranulation. Summary data for the numbers of PD-1⁺ LCMV-specific CD8⁺ T cells producing IFNγ and TNFα, IFNγ and IL-2, and IFNγ plus degranulation (CD107a⁺) are shown as a function of the three clusters in the different treatment groups. **e**, Antigen-independent effector function. Spleen cells were stimulated with IL-12 and IL-18 (20 ng ml^{-1} each) for 6 h without any viral peptides. Cells were then stained for surface markers, including D^bGP33-specific tetramer, fixed and subsequently intracellularly stained for IFNγ. Summary data for the numbers of LCMV-specific CD8⁺ T cells producing IFNγ⁺ in an antigen-independent manner as a function of the three clusters in the various treatment groups. **f**, The chemotaxis index for CXCL9 and CXCL10. Sorted PD-1⁺CD8⁺ T cells obtained from pooled spleens of chronically infected mice treated for 2 weeks by each treatment were tested for chemotaxis to CXCL9 and CXCL10. For **a**–**e**, the results were pooled from 2–4 experiments with 1–8 mice per group in each experiment. Data are mean ± s.d. (**b**), mean ± s.e.m. (**d** and **e**) or geometric mean ± 95% CI (**f**). *P* values are shown; statistical comparisons were performed using Kruskal–Wallis tests with Dunn's multiple-comparison test (**d**–**f**).

after acute viral infection. This epigenetic modification most likely represents the generation of new $CD8^+$ T_{eff} cells from the TCF1⁺ stem-like $CD8^+$ T cells after combination therapy as opposed to reprogramming exhausted $CD8^+$ T cells.

PD-1 blockade at target site is crucial for viral reduction

One important question is why does IL-2 monotherapy have a minimal effect in reducing the viral load during chronic LCMV infection despite expanding the virus-specific $CD8^+$ T cells and bringing about qualitative changes in the $CD8^+$ T cells similar to what was seen after PD-1 + IL-2 combination therapy. Our previous studies showed that expression of PD-L1 on LCMV-infected cells may inhibit the $CD8^+$ T_{eff} cells from eliminating the infected cell[31]. Other studies using tumour models have also made similar observations[32,33]. Thus, we hypothesized that, after IL-2 monotherapy, the viral control was compromised despite the increased numbers of $CD8^+$ T cells owing to PD-L1 expression at the target site. To test this hypothesis, we designed a treatment regimen in which LCMV chronically infected mice were treated with IL-2 first for 10 days to expand the LCMV-specific $CD8^+$ T cells and then PD-1 blockade was performed for just 3 days starting at day 10. The control group of chronically infected mice received IL-2 only from days 0–13 (Extended Data Fig. 7a). These two groups of mice were then analysed on day 14 for LCMV-specific $CD8^+$ T cell responses and viral control. There were no differences in the numbers of LCMV-specific $CD8^+$ T cells in the spleen, liver and lungs of the two groups of mice (Extended Data Fig. 7b). This was the expected result as most of the expansion of $CD8^+$ T cells would have already occurred during the first 10 days, and this would have been driven by IL-2 therapy alone. The key question now was whether PD-1 blockade at the tail-end of IL-2 therapy would result in any viral control. This was indeed the case. Chronically infected mice treated with anti-PD-L1 antibodies from day 10–13 had significantly lower levels of virus in all three tissues (spleen, liver and lungs) examined compared with mice that received IL-2 only (Extended Data Fig. 7c). This is clearly consistent with PD-1 blockade at the target site enhancing viral control. To further expand on this, we examined whether there were any pathological changes in the liver after anti-PD-L1 treatment. We found that chronically infected mice that received the late PD-1 blockade had significantly increased levels of liver enzyme in the serum and showed a higher pathology score and an increased number of TUNEL-positive cells in the liver compared with the IL-2-only group (Extended Data Fig. 7d–f). Taken together, these results highlight the importance of blocking the PD-1/PD-L1 inhibitory pathway at the target site for effective viral control.

PD-1 + IL-2 improves the $CD8^+$ T_{eff}/$CD4^+$ T_{reg} cell ratio

Treatment of mice chronically infected with LCMV with IL-2 alone or PD-1 + IL-2 combination therapy increases the number

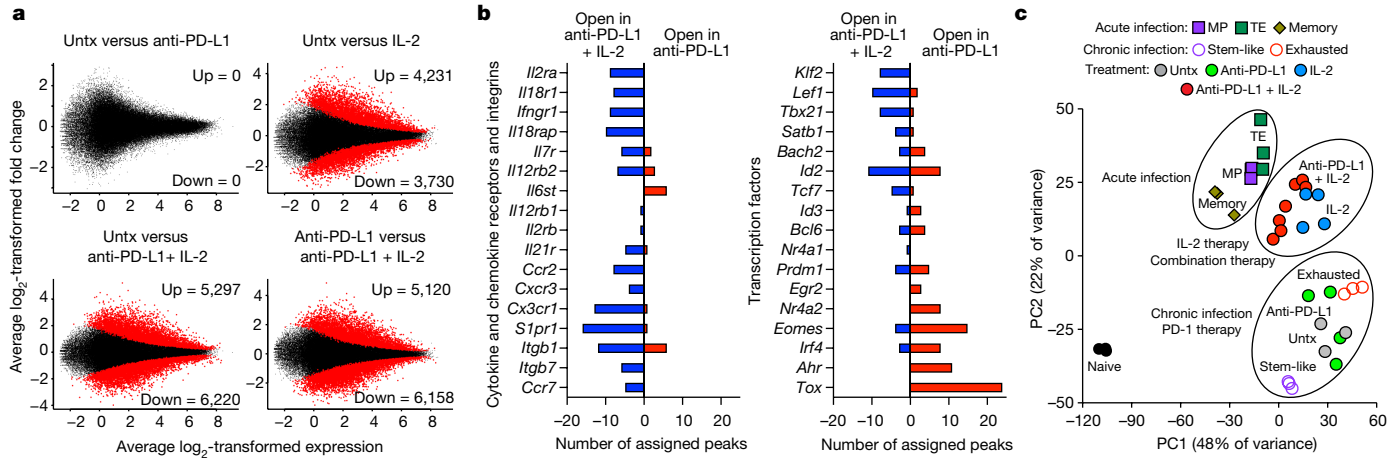

Fig. 4 | Epigenetic signatures of LCMV-specific CD8$^+$ T cells generated by IL-2 or PD-1 + IL-2 combination therapy are distinct from that by PD-1 monotherapy during chronic infection. a, *MA* plots for differentially accessible regions in LCMV-specific D^{b}GP33$^+$CD8$^+$ T cells examined using ATAC-seq after PD-1 and IL-2 therapy and PD-1 + IL-2 combination therapy. Down, downregulated (closed); up, upregulated (open). **b**, Gene annotations of differentially accessible distal regulatory regions in D^{b}GP33$^+$CD8$^+$ T cells of mice treated with anti-PD-L1 and PD-1 + IL-2 combination therapy. The number of differentially open gene regulatory regions for genes of functional importance in D^{b}GP33$^+$CD8$^+$ T cells after PD-1 monotherapy versus PD-1 + IL-2 combination therapy is shown. **c**, PCA plot of ATAC-seq analysis of naive CD8$^+$ T cells and the various LCMV-specific CD8$^+$ T cell subsets generated during acute and chronic infection, and the D^{b}GP33$^+$CD8$^+$ T cells generated after PD-1 monotherapy, IL-2 treatment or the combination therapy. The results were pooled from three ATAC-seq experiments with $n = 12–18$ for untreated mice or $n = 1–3$ for treatment samples per group in each experiment. The ATAC-seq data for naive, acute (memory precursor (MP), terminal effector (TE) and memory) and chronic (stem-like and exhausted) are from our previous study[30].

of FOXP3$^+$CD4$^+$ regulatory T (T_{reg}) cells. However, the increase in LCMV-specific CD8$^+$ T cells is tenfold higher after PD-1 + IL-2 combination therapy resulting in notably different ratios of LCMV-specific CD8$^+$ T cells to CD4$^+$ T_{reg} cells after IL-2 monotherapy versus PD-1 + IL-2 combination therapy. This favourable CD8$^+$ T_{eff} cell/CD4$^+$ T_{reg} ratio after PD-1 + IL-2 combination therapy could also contribute to better viral control (Extended Data Fig. 8a–d) and has implications for cancer immunotherapy in which CD4$^+$ T_{reg} cells are known to have an important role[34].

CD25 is important for synergy between IL-2 and PD-1

The notable synergy between PD-1 blockade and IL-2 during chronic LCMV infection was achieved using the natural IL-2 cytokine (IL-2(WT)). Many of the ongoing human clinical trials combining PD-1 blockade with IL-2 to treat patients with cancer use genetically engineered or modified forms of IL-2 that do not bind to CD25[2,3]. It was therefore of interest to determine whether CD25 engagement has a role in the synergistic effects that we have observed in the LCMV model.

We first examined how CD25 expression changes after the various treatments and which chronic CD8$^+$ T cell subsets express CD25. To address this, we sorted the PD-1$^+$ stem-like CD8$^+$ T cells and the more differentiated CD8$^+$ T cells from chronically infected mice, and transferred them into infection-matched congenically distinct mice so we could track the donor CD8$^+$ T cells. Groups of these chronically infected mice were either left untreated, or treated with PD-1 blockade alone, IL-2 alone or the combination therapy. Note that neither the stem-like CD8$^+$ T cell population nor the terminally differentiated CD8$^+$ T cells expressed any detectable levels of CD25 at the time of transfer. However, after the adoptive transfer, the stem-like CD8$^+$ T cells that received IL-2 alone or PD-1 + IL-2 combination therapy underwent expansion and also expressed CD25. Interestingly, PD-1 blockade alone resulted in increased proliferation and differentiation of the stem-like CD8$^+$ T cells but there was minimal to no CD25 detectable on this expanded population. The more terminally differentiated (exhausted) CD8$^+$ T cells did not expand in response to any of the treatments and did not upregulate CD25 expression (Extended Data Fig. 9a–d). These results show that the expanded population of CD25$^+$CD8$^+$ T cells is derived from the PD-1$^+$TCF1$^+$ stem-like CD8$^+$ T cells and that CD25 upregulation is selectively seen only after IL-2 treatment or PD-1 + IL-2 combination therapy.

Having established the origin of the CD25$^+$CD8$^+$ T cells in the above experiment, we next examined in more detail the kinetics of CD25 expression on LCMV-specific CD8$^+$ T cells in chronically infected mice after PD-1 blockade, IL-2 treatment or combination therapy. A small percentage (mean, 15%) of LCMV-specific CD8$^+$ T cells started expressing CD25 at day 3 after combination therapy and, by day 6 after treatment, the majority (mean, 64%) of tetramer-positive CD8$^+$ T cells were proliferating and expressing CD25. A similar trend but with slightly lower numbers (mean, 35%) was observed in mice that received IL-2 treatment only. By contrast, PD-1 blockade alone increased the number of proliferating virus-specific CD8$^+$ T cells at day 6 but these cells did not express detectable levels of CD25 (Extended Data Fig. 9e–i). We also examined the expression of CD122 and CD132, the β and γ chains of the IL-2 receptor. Minimal changes were seen in expression of CD122 or CD132 after PD-1 monotherapy but there were significant increases in the expression of both CD122 and CD132 after IL-2 treatment alone and especially after the combination therapy (Extended Data Fig. 9j–o). Thus, PD-1 + IL-2 combination therapy resulted in the upregulation of all three chains (CD25, CD122, CD132) to form the high-affinity trimeric IL-2 receptor on the proliferating and differentiating LCMV-specific CD8$^+$ T cells[35].

It was important to determine whether CD25 engagement by IL-2 was essential for the observed synergy between PD-1 blockade and IL-2 during chronic LCMV infection. To address this question, a blocking and non-depleting anti-CD25 antibody[36] was administered during the combination therapy to block the interaction between IL-2 and CD25 (Fig. 5a). Treatment with this anti-CD25 antibody almost completely abrogated the synergy between IL-2 and PD-1 therapy. The increased expansion of LCMV D^{b}GP33-specific CD8$^+$ T cells was not observed, the increased poly-functionality of the virus-specific CD8$^+$ T cells was reduced and the phenotypic changes associated with the generation of acute-infection-like CD8$^+$ T_{eff} cells were no longer seen. As a consequence, the superior viral control by PD-1 + IL-2 combination therapy over PD-1 monotherapy was lost when the interaction between CD25 and IL-2 was prevented (Fig. 5b–e). These findings show that CD25 engagement is critical for the optimal synergistic effect of PD-1 + IL-2 combination therapy.

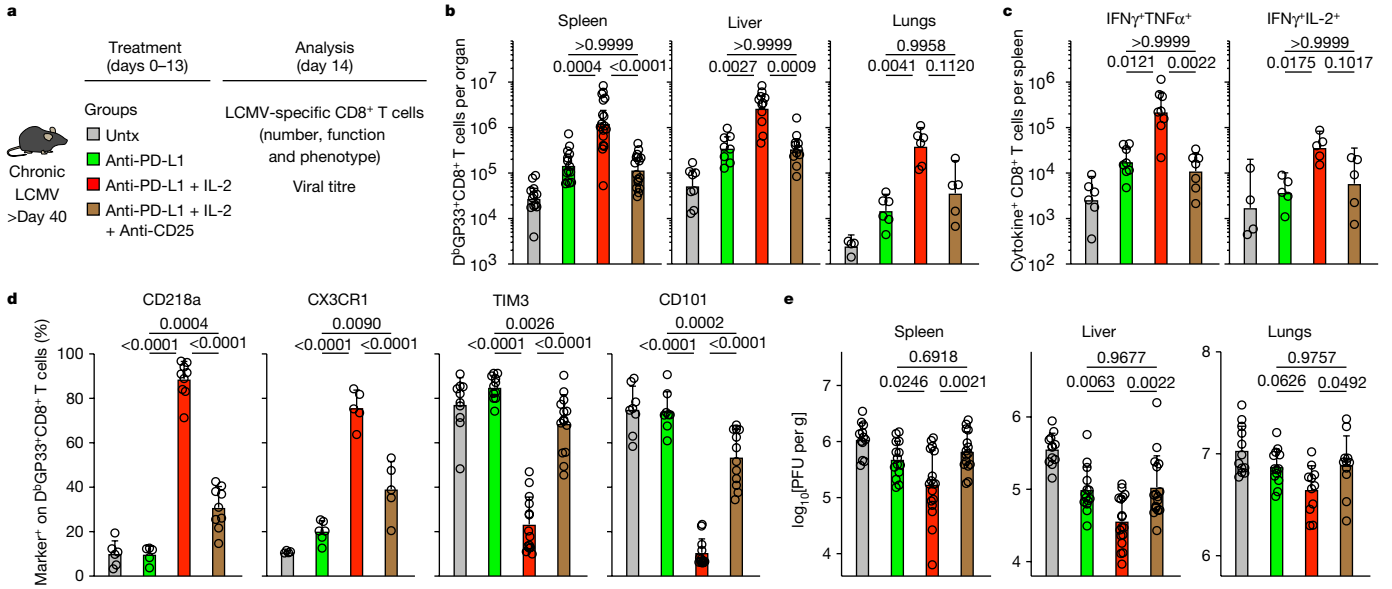

Fig. 5 | CD25 blockade abrogates the synergy between IL-2 and PD-1 blockade. a, Chronically infected mice were left untreated, or were treated with anti-PD-L1 antibodies or combination therapy with anti-PD-L1 plus IL-2 for 2 weeks. One additional group was given the combination therapy plus a blocking anti-CD25 (PC61-N297Q) antibody for 2 weeks. The LCMV-specific CD8$^+$ T cell response and viral titre were analysed on day 14. The colour key in **a** applies to **b**–**e**. **b**, LCMV-specific CD8$^+$ T cell responses. The numbers of D^{b}GP33$^+$CD8$^+$ T cells in the indicated tissues for all four groups of mice are shown. **c**, The numbers of IFNγ$^+$, IFNγ$^+$TNFα$^+$ and IFNγ$^+$IL-2$^+$CD8$^+$ T cells in the different groups of mice. Spleen cells were stimulated with pools of LCMV-specific peptides for 5 h and analysed by intracellular cytokine staining. **d**, The phenotype of D^{b}GP33$^+$CD8$^+$ T cells from the indicated treatment groups. **e**, Viral titre in the indicated tissues in the four groups of mice. The results were pooled from 2–6 experiments with at least 4 mice per group. Data are geometric mean ± 95% CI (**b** and **c**) or mean ± s.d. (**d** and **e**). *P* values are shown; statistical comparisons were performed using Kruskal–Wallis tests with Dunn's multiple-comparison test (**b** and **c**) or one-way analysis of variance (ANOVA) with Tukey's multiple-comparison test (**d** and **e**).

PD-1 combination therapy with IL-2(WT) versus IL-2(V)

Another approach to the above question is to use a mutated version of IL-2 (IL-2(V)) that does not bind to CD25 and examine how this IL-2(V) compares with the natural IL-2 cytokine (IL-2(WT)) in combination therapy with PD-1 blockade in LCMV chronically infected mice. The IL-2(V) that we used in these studies was genetically modified to prevent binding to CD25 without affecting IL-2 structure or the interaction with IL-2Rβγ[37]. The experimental set-up comparing PD-1 combination therapy with IL-2(WT) or IL-2(V) is shown in Fig. 6a. Similar to our results with the CD25 blockade experiments, we found that IL-2(V) combination therapy did not result in significantly increased numbers of LCMV-specific CD8$^+$ T cells compared with PD-1 monotherapy in multiple tissues. This was in contrast to the highly significant increases seen in virus-specific CD8$^+$ T cells after PD-1 combination therapy with IL-2(WT) (Fig. 6b and Extended Data Fig. 10a,b). We also compared the transcriptional profile of LCMV-specific CD8$^+$ T cells isolated from mice given combination therapy with IL-2(V) versus IL-2(WT). Notably, the distinct gene signature observed after combination therapy with IL-2(WT) was lost with IL-2(V). IL-2(V) combination therapy also did not induce the key qualitative changes in LCMV-specific CD8$^+$ T cells based on expression of phenotypic markers and their ability to make various cytokines compared with PD-1 combination therapy with IL-2(WT). Importantly, no improved viral control over PD-1 therapy was observed after IL-2(V) combination therapy (Fig. 6c–f and Extended Data Fig. 10c,d). Thus, taken together, the experiments with CD25 blockade and comparing IL-2(V) versus IL-2(WT) clearly show that CD25 engagement has a substantial and essential role in the synergistic effects of IL-2 in combination therapy with PD-1 blockade.

Note that IL-2(V) was biologically active in vivo in expanding CD8$^+$ T cells but did not target the right CD8$^+$ T cell population. There were significant increases in the number of CD8$^+$ T cells after PD-1 combination therapy with IL-2(V) but this was predominantly due to the expansion of PD-1-negative CD8$^+$ T cells and there was no increase in the number of PD-1$^+$CD8$^+$ T cells above what was seen with PD-1 blockade alone. By contrast, PD-1 combination therapy with IL-2(WT) resulted in the selective expansion of PD-1-positive CD8$^+$ T cells—this is where all the LCMV-specific CD8$^+$ T cells are found (Extended Data Fig. 11a–g). The most likely explanation for these results is that, as the vast majority of CD8$^+$ T cells in these mice are not virus-specific and all of these CD8$^+$ T cells express the β (CD122) and γ (CD132) chains of the IL-2 receptor, the IL-2(V) cytokine is being soaked up by this large population of non-virus-specific CD8$^+$ T cells, whereas the high-affinity trimeric IL-2 receptor (CD25–CD122–CD132) that is expressed on the virus-specific CD8$^+$ T cells would selectively capture the IL-2(WT) cytokine[35,38]. The substantial upregulation of CD25 in particular and also CD122 and CD132 on LCMV-specific CD8$^+$ T cells is seen only after IL-2(WT) therapy. IL-2(V) treatment results in a slight increase in CD122 expression but does not change CD25 and CD132 expression (Extended Data Fig. 12a–f). Thus, the IL-2(V) is diluted out while the IL-2(WT) is being selectively captured by the PD-1$^+$ virus-specific CD8$^+$ T cells. If appropriate targeting strategies are used with IL-2(V), then this could be an effective and safe approach for immunotherapy. This issue is addressed in an accompanying paper[39].

All of the results that we have shown so far used the stringent LCMV clone 13 model of life-long chronic infection in the absence of LCMV-specific CD4$^+$ T cells. We next compared the effects of PD-1 + IL-2(WT) versus PD-1 + IL-2(V) combination therapy in LCMV chronically infected mice containing virus-specific CD4$^+$ T cells. The results of these experiments are shown in Extended Data Fig. 13. We found that the synergistic increase in LCMV-specific CD8$^+$ T cells was observed only in mice that received PD-1 combination therapy with the IL-2(WT) cytokine. There was minimal to no synergy between IL-2(V) cytokine and PD-1 blockade. Moreover, the phenotypic and functional changes in LCMV-specific CD8$^+$ T cells that reflect better effector function and decreased exhaustion were seen in mice treated with anti-PD-L1 and IL-2(WT) and not in combination with IL-2(V). Consistent with these quantitative and qualitative changes in LCMV-specific CD8$^+$ T

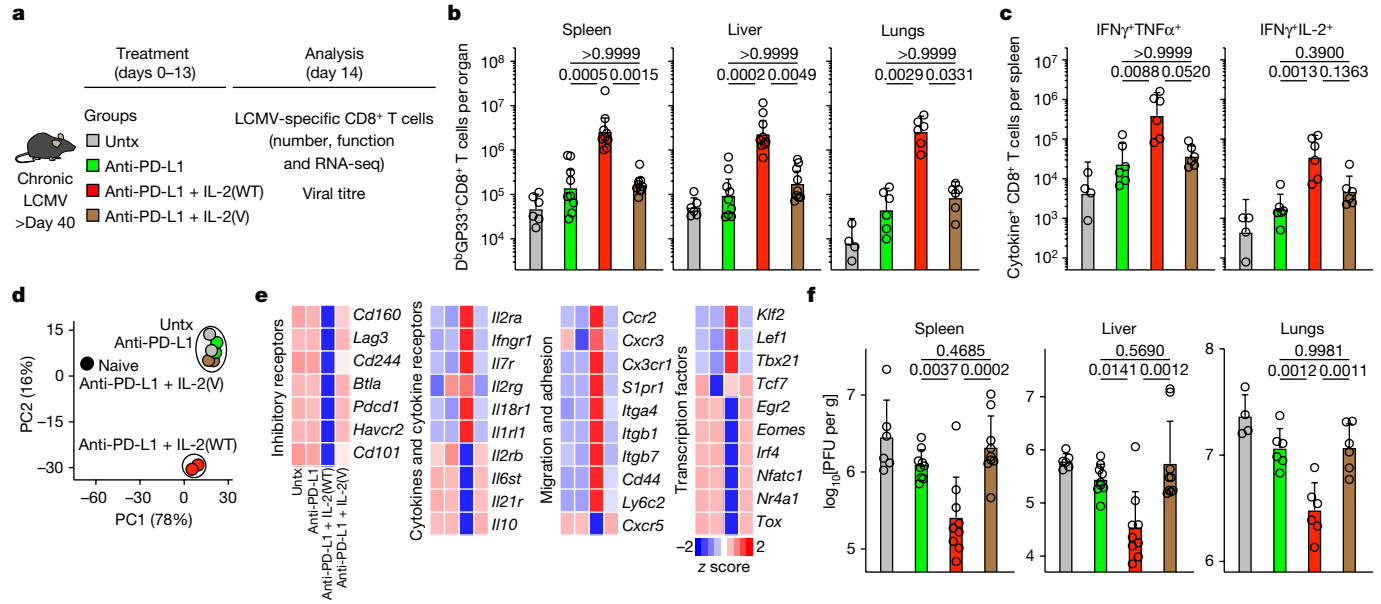

Fig. 6 | CD25 engagement by therapeutic IL-2 is crucial for the efficacy of PD-1 + IL-2 combination therapy. a, LCMV chronically infected mice (>40 days after infection) were left untreated, or were treated with anti-PD-L1 antibodies, anti-PD-L1 plus IL-2(WT) or anti-PD-L1 plus IL-2(V) (modified IL-2 with abolished CD25 binding) for 2 weeks. The colour key in **a** applies to **b**–**d** and **f**. **b**, LCMV-specific CD8$^+$ T cell responses. The numbers of LCMV-specific D^{b}GP33$^+$CD8$^+$ T cells in the indicated tissues after the various treatments are shown. **c**, The numbers of IFNγ$^+$TNFα$^+$ and IFNγ$^+$IL-2$^+$ LCMV-specific CD8$^+$ T cells in the four groups. Spleen cells were stimulated with pools of LCMV-specific peptides for 5 h and analysed by intracellular cytokine staining. **d**,**e**, LCMV-specific D^{b}GP33$^+$CD8$^+$ T cells were sorted from the spleens of LCMV chronically infected mice after various treatments and analysed using RNA-seq. Naive CD44^{low}CD8$^+$ T cells from uninfected mice were also included in the analysis. **d**, PCA plot for naive (CD44^{low}) and D^{b}GP33$^+$CD8$^+$ T cells generated by the different treatments. **e**, The mean relative expression of key specific genes in D^{b}GP33$^+$CD8$^+$ T cells generated after the various treatments. **f**, The viral titre in the indicated tissues in the four groups of mice. The results were pooled from 2–3 experiments with 2–3 mice per group in each experiment. Data are geometric mean ± 95% CI (**b** and **c**) or mean ± s.d. (**f**). *P* values are shown; statistical comparisons were performed using Kruskal–Wallis tests with Dunn's multiple-comparison test (**b** and **c**) or one-way ANOVA with Tukey's multiple-comparison test (**f**).

cells, the most effective viral control was seen in mice that received PD-1 + IL-2(WT) combination therapy (Extended Data Fig. 13b–e). This model of LCMV chronic infection with CD4$^+$ T cell help also enabled us to examine the effect of PD-1 + IL-2 combination therapy on LCMV-specific CD4$^+$ T cells. A significant increase in LCMV-specific CD4$^+$ T cells with the T helper type 1 (Th1) phenotype was observed only in mice receiving PD-1 blockade plus the IL-2(WT) cytokine (Extended Data Fig. 13f). Thus, in both CD4$^+$ T cell helped and unhelped models of LCMV chronic infection, combination therapy with PD-1 + IL-2(WT) is superior to PD-1 + IL-2(V).

Discussion

Here we examined how IL-2 synergizes with PD-1-directed immunotherapy during chronic LCMV infection. We make the following points: first, we showed that the more effective viral control seen after PD-1 + IL-2 combination therapy compared with PD-1 monotherapy is mediated by the CD8$^+$ T cell response. We then identified the virus-specific CD8$^+$ T cells that proliferate and respond to the combination therapy and show that these are the same lymphoid resident PD-1$^+$TCF1$^+$ resource CD8$^+$ T cells that also respond to PD-1 blockade. However, the combination therapy substantially changes the differentiation program of these stem-like CD8$^+$ T cells and results in the generation of transcriptionally and epigenetically distinct CD8$^+$ T_{eff} cells that resemble highly functional CD8$^+$ T_{eff} cells seen after an acute viral infection. Note that this striking modification of the CD8$^+$ T cell exhaustion program after PD-1 + IL-2 combination therapy is primarily due to IL-2 signals changing the CD8$^+$ T_{eff} cell differentiation program from the PD-1$^+$TCF1$^+$ stem-like CD8$^+$ T cells as opposed to reprogramming terminally differentiated exhausted CD8$^+$ T cells. This is also consistent with our finding that the terminally differentiated CD8$^+$ T cells did not expand after IL-2 alone or PD-1 + IL-2 combination therapy (Fig. 1 and Extended Data Fig. 2). This ability to modify the differentiation program and generate better CD8$^+$ T_{eff} cells could be the underlying mechanism for the notable synergy seen between IL-2 therapy and PD-1 blockade. We also highlight the importance of blocking the PD-1/PD-L1 inhibitory pathway at the target site for effective viral control[31]. Expanding the CD8$^+$ T cell population and generating better effector cells is important but it is also critical to block PD-1 inhibitory signals at the target site for optimal immunotherapy. Finally, we show that CD25 engagement with IL-2 has an important and essential role in the observed synergy between IL-2 cytokine and PD-1 blockade. Either blocking CD25 with an antibody or using a mutated version of IL-2 that does not bind to CD25 (but still binds to CD122–CD132) almost completely abrogated the synergistic effects seen after PD-1 + IL-2 combination therapy. There is considerable interest in using PD-1 + IL-2 combination therapy in patients with cancer. Several clinical trials are ongoing and many of these trials are using modified or genetically engineered forms of IL-2 that do not bind to CD25[2,3]. The recent clinical trial using anti-PD-1 antibodies in combination with pegylated IL-2 with decreased CD25 binding has shown disappointing results[40]. Our studies in the chronic LCMV model enabled us to dissect the underlying mechanisms of how IL-2 therapy synergizes with PD-1 blockade. This information will be valuable in providing guidelines for optimizing PD-1 + IL-2 therapy in human clinical trials for chronic viral infections and cancer.

Online content

Any methods, additional references, Nature Research reporting summaries, source data, extended data, supplementary information, acknowledgements, peer review information; details of author contributions and competing interests; and statements of data and code availability are available at https://doi.org/10.1038/s41586-022-05257-0.

1. West, E. E. et al. PD-L1 blockade synergizes with IL-2 therapy in reinvigorating exhausted T cells. *J. Clin. Invest.* **123**, 2604–2615 (2013).
2. Pol, J. G., Caudana, P., Paillet, J., Piaggio, E. & Kroemer, G. Effects of interleukin-2 in immunostimulation and immunosuppression. *J. Exp. Med.* **217**, e20191247 (2019).
3. Overwijk, W. W., Tagliaferri, M. A. & Zalevsky, J. Engineering IL-2 to give new life to T cell immunotherapy. *Annu. Rev. Med.* **72**, 281–311 (2021).
4. Hashimoto, M. et al. CD8 T cell exhaustion in chronic infection and cancer: opportunities for interventions. *Annu. Rev. Med.* **69**, 301–318 (2018).
5. McLane, L. M., Abdel-Hakeem, M. S. & Wherry, E. J. CD8 T cell exhaustion during chronic viral infection and cancer. *Annu. Rev. Immunol.* **37**, 457–495 (2019).
6. Leonard, W. J., Lin, J. X. & O'Shea, J. J. The γ_c family of cytokines: basic biology to therapeutic ramifications. *Immunity* **50**, 832–850 (2019).
7. Gillis, S., Ferm, M. M., Ou, W. & Smith, K. A. T cell growth factor: parameters of production and a quantitative microassay for activity. *J. Immunol.* **120**, 2027–2032 (1978).
8. He, R. et al. Follicular CXCR5-expressing $CD8^+$ T cells curtail chronic viral infection. *Nature* **537**, 412–428 (2016).
9. Hudson, W. H. et al. Proliferating transitory T cells with an effector-like transcriptional signature emerge from PD-1+ stem-like $CD8^+$ T cells during chronic infection. *Immunity* **51**, 1043–1058 (2019).
10. Im, S. J. et al. Defining $CD8^+$ T cells that provide the proliferative burst after PD-1 therapy. *Nature* **537**, 417–421 (2016).
11. Im, S. J., Konieczny, B. T., Hudson, W. H., Masopust, D. & Ahmed, R. PD-1^+ stemlike CD8 T cells are resident in lymphoid tissues during persistent LCMV infection. *Proc. Natl Acad. Sci. USA* **117**, 4292–4299 (2020).
12. Leong, Y. A. et al. $CXCR5^+$ follicular cytotoxic T cells control viral infection in B cell follicles. *Nat. Immunol.* **17**, 1187–1196 (2016).
13. Utzschneider, D. T. et al. T cell factor 1-expressing memory-like $CD8^+$ T cells sustain the immune response to chronic viral infections. *Immunity* **45**, 415–427 (2016).
14. Zander, R. et al. $CD4^+$ T cell help is required for the formation of a cytolytic $CD8^+$ T cell subset that protects against chronic infection and cancer. *Immunity* **51**, 1028–1042 (2019).
15. Seo, H. et al. TOX and TOX2 transcription factors cooperate with NR4A transcription factors to impose $CD8^+$ T cell exhaustion. *Proc. Natl Acad. Sci. USA* **116**, 12410–12415 (2019).
16. Wherry, E. J. et al. Molecular signature of $CD8^+$ T cell exhaustion during chronic viral infection. *Immunity* **27**, 670–684 (2007).
17. Hudson, W. H. et al. Expression of novel long noncoding RNAs defines virus-specific effector and memory $CD8^+$ T cells. *Nat. Commun.* **10**, 196 (2019).
18. Joshi, N. S. et al. Inflammation directs memory precursor and short-lived effector $CD8^+$ T cell fates via the graded expression of T-bet transcription factor. *Immunity* **27**, 281–295 (2007).
19. Kaech, S. M. et al. Selective expression of the interleukin 7 receptor identifies effector CD8 T cells that give rise to long-lived memory cells. *Nat. Immunol.* **4**, 1191–1198 (2003).
20. Sarkar, S. et al. Functional and genomic profiling of effector CD8 T cell subsets with distinct memory fates. *J. Exp. Med.* **205**, 625–640 (2008).
21. Chow, M. T. et al. Intratumoral activity of the CXCR3 chemokine system is required for the efficacy of anti-PD-1 therapy. *Immunity* **50**, 1498–1512 (2019).
22. Hickman, H. D. et al. CXCR3 chemokine receptor enables local $CD8^+$ T cell migration for the destruction of virus-infected cells. *Immunity* **42**, 524–537 (2015).
23. Pauken, K. E. et al. Epigenetic stability of exhausted T cells limits durability of reinvigoration by PD-1 blockade. *Science* **354**, 1160–1165 (2016).
24. Sen, D. R. et al. The epigenetic landscape of T cell exhaustion. *Science* **354**, 1165–1169 (2016).
25. Buenrostro, J. D., Giresi, P. G., Zaba, L. C., Chang, H. Y. & Greenleaf, W. J. Transposition of native chromatin for fast and sensitive epigenomic profiling of open chromatin, DNA-binding proteins and nucleosome position. *Nat. Methods* **10**, 1213–1218 (2013).
26. McLean, C. Y. et al. GREAT improves functional interpretation of *cis*-regulatory regions. *Nat. Biotechnol.* **28**, 495–501 (2010).
27. Alfei, F. et al. TOX reinforces the phenotype and longevity of exhausted T cells in chronic viral infection. *Nature* **571**, 265–269 (2019).
28. Khan, O. et al. TOX transcriptionally and epigenetically programs $CD8^+$ T cell exhaustion. *Nature* **571**, 211–218 (2019).
29. Scott, A. C. et al. TOX is a critical regulator of tumour-specific T cell differentiation. *Nature* **571**, 270–274 (2019).
30. Jadhav, R. R. et al. Epigenetic signature of PD-1^+ $TCF1^+$ CD8 T cells that act as resource cells during chronic viral infection and respond to PD-1 blockade. *Proc. Natl Acad. Sci. USA* **116**, 14113–14118 (2019).
31. Mueller, S. N. et al. PD-L1 has distinct functions in hematopoietic and nonhematopoietic cells in regulating T cell responses during chronic infection in mice. *J. Clin. Invest.* **120**, 2508–2515 (2010).
32. Juneja, V. R. et al. PD-L1 on tumor cells is sufficient for immune evasion in immunogenic tumors and inhibits CD8 T cell cytotoxicity. *J. Exp. Med.* **214**, 895–904 (2017).
33. Lau, J. et al. Tumour and host cell PD-L1 is required to mediate suppression of anti-tumour immunity in mice. *Nat. Commun.* **8**, 14572 (2017).
34. Plitas, G. & Rudensky, A. Y. Regulatory T cells in cancer. *Annu. Rev. Cancer Biol.* **4**, 459–477 (2020).
35. Malek, T. R. & Castro, I. Interleukin-2 receptor signaling: at the interface between tolerance and immunity. *Immunity* **33**, 153–165 (2010).
36. Huss, D. J. et al. Anti-CD25 monoclonal antibody Fc variants differentially impact regulatory T cells and immune homeostasis. *Immunology* **148**, 276–286 (2016).
37. Klein, C. et al. Cergutuzumab amunaleukin (CEA-IL2v), a CEA-targeted IL-2 variant-based immunocytokine for combination cancer immunotherapy: overcoming limitations of aldesleukin and conventional IL-2-based immunocytokines. *Oncoimmunology* **6**, e1277306 (2017).
38. Su, E. W. et al. IL-2Rα mediates temporal regulation of IL-2 signaling and enhances immunotherapy. *Sci. Transl. Med.* **7**, 311ra170 (2015).
39. Codarri Deak, L. et al. PD-1-*cis*-IL-2R agonism yields better effectors from stem-like CD8 T cells. *Nature* https://doi.org/10.1038/s41586-022-05192-0 (2022).
40. Bristol Myers Squibb and Nektar announce update on phase 3 PIVOT IO-001 trial evaluating bempegaldesleukin (BEMPEG) in combination with Opdivo (nivolumab) in previously untreated unresectable or metastatic melanoma (Businesswire, 2022); https://www.businesswire.com/news/home/20220313005021/en/Bristol-Myers-Squibb-and-Nektar-Announce-Update-on-Phase-3-PIVOT-IO-001-Trial-Evaluating-Bempegaldesleukin-BEMPEG-in-Combination-with-Opdivo-nivolumab-in-Previously-Untreated-Unresectable-or-Metastatic-Melanoma

Methods

Mice, virus and infection

Female C57BL/6J and CD45.1 congenic mice (aged 6–8 weeks) were purchased from the Jackson Laboratory. LCMV chronically infected mice were generated as follows. Mice were transiently depleted of $CD4^+$ T cells by injecting them with 300 μg of rat anti-mouse CD4 antibody (GK1.5, BioXCell) intraperitoneally (i.p.) 2 days before infection and again on the day of infection; the mice were then infected with 2×10^6 plaque-forming units of LCMV clone 13 intravenously through the tail vein. For examining the therapeutic effects of PD-1 + IL-2 therapy on $CD8^+$ T cells in the presence of LCMV-specific $CD4^+$ T cells, the mice were infected with LCMV clone 13 without transient $CD4^+$ T cell depletion. Titres of virus were determined by plaque assay on Vero E6 cells (ATCC). Vero E6 cells were neither authenticated nor tested for mycoplasma contamination. No statistical methods were used to predetermine sample size. LCMV chronically infected mice were randomly assigned to experimental groups and investigators were not blinded to group allocation during experimental setup, data collection or analysis. All animal experiments were performed in accordance with National Institutes of Health and the Emory University Institutional Animal Care and Use Committee guidelines. Mice were housed under the following conditions: light cycle, 07:00 on and 19:00 off; temperature of between 68–72 °F; humidity of between 30–70 g m^{-3}.

Lymphocyte isolation

Lymphocytes were isolated from the blood, spleen, liver and lungs as described previously[41]. In brief, spleens were dissociated by passing them through a 70 μm cell strainer (Corning). Livers were perfused with pre-cooled PBS and homogenized by mechanical disruption. Lungs were treated with 1.3 mM EDTA in HBSS for 30 min at 37 °C with shaking at 200 rpm, followed by treatment with 150 U ml^{-1} collagenase (Thermo Fisher Scientific) in RPMI 1640 medium containing 5% FBS, 1 mM $MgCl_2$ and 1mM $CaCl_2$ for 60 min at 37 °C with shaking at 200 rpm. Collagenase-treated lung tissues were homogenized and filtered through a 70 μm cell strainer. Lymphocytes from livers and lungs were purified by a 44–67% Percoll gradient (800*g* at 20 °C for 20 min).

Reagents, flow cytometry and in vitro stimulations

All antibodies for flow cytometry were purchased from BD Biosciences, BioLegend, Thermo Fisher Scientific, Cell Signaling Technology and R&D Systems, and were used at the following dilutions: anti-Bcl-6 PE, 1:20; anti-CD4 BUV496, 1:500; anti-CD4 BUV563, 1:500; anti-CD4 FITC, 1:500; anti-CD4 V500, 1:500; anti-CD4 BV605, 1:500; anti-CD4 PE-Cy7, 1:500; anti-CD4 APC-eFluor 780, 1:500; anti-CD8a BUV496, 1:100; anti-CD8a BUV563, 1:100; anti-CD8a BV421, 1:150; anti-CD8a BV605, 1:100; anti-CD8a PerCP, 1:100; anti-CD8a APC, 1:100; anti-CD8b.2 BV421, 1:200; anti-CD19 BUV563, 1:150; anti-CD19 BV510, 1:150; anti-CD19 BV605, 1:150; anti-CD19 PE-Cy7, 1:150; anti-CD19 APC-eFluor 780, 1:150; anti-CD25 BV421, 1:100; anti-CD25 PE, 1:100; anti-CD25 BB700, 1:100; anti-CD25 PE-Cy7, 1:100; anti-CD28 PE, 1:100; anti-CD29 eFluor 450, 1:100; anti-CD44 BUV805, 1:500; anti-CD44 FITC, 1:500; anti-CD44 Alexa Fluor 700, 1:100; anti-CD45.2 BV421, 1:100; anti-CD45.2 APC, 1:100; anti-CD49d PE, 1:100; anti-CD62L BV650, 1:100; anti-CD69 PE-Cy7, 1:100; anti-CD73 BV605, 1:100; anti-CD101 PE-Cy7, 1:100; anti-CD101 APC, 1:100; anti-CD107a Alexa Fluor 488, 1:200; anti-CD119 BV421, 1:100; anti-CD122 PE, 1:100; anti-CD127 PE, 1:100; anti-CD132 BV421, 1:100; anti-CD132 PE, 1:100; anti-CD160 BV421, 1:100; anti-CD218a PE, 1:100; anti-CD218a PerCP-eFluor 710, 1:100; anti-CD218a PE-Cy7, 1:100; anti-CD223 BV421, 1:100; anti-CD226 PE-Cy7, 1:100; anti-CXCR3 BV480, 1:100; anti-CXCR3 PE-Cy7, 1:100; anti-CXCR5 BV421, 1:50; anti-CXCR5 PE-Dazzle, 1:50; anti-CX3CR1 BV785, 1:500; anti-CX3CR1 PE, 1:500; anti-BTLA PE, 1:100; anti-EOMES PE-Cy7, 1:100; anti-FOXP3 PE-Cy7, 1:250; anti-granzyme A PE, 1:100; anti-granzyme B BV421, 1:20; anti-granzyme B PE, 1:20; anti-ICOS PE, 1:100; anti-IL-2 PE, 1:100; anti-IFNγ BV421, 1:100; anti-IFNγ BV480, 1:100; anti-IFNγ BV711, 1:100; anti-IFNγ APC, 1:100; anti-Ki-67 FITC, 1:20; anti-Ly-6C BV421, 1:500; anti-Ly-6C R718, 1:500; anti-PD-1 BV421, 1:100; anti-PD-1 BV605, 1:100; anti-PD-1 BV711, 1:100; anti-PD-1 PE, 1:100; anti-PD-1 APC, 1:100; anti-SLAMF6 BUV737, 1:100; anti-TCF1 Alexa Fluor 488, 1:50; anti-TCF1 PE, 1:100; anti-TIM3 BUV395, 1:100; anti-TIM3 Alexa Fluor 488, 1:20; anti-TIM3 PE, 1:20; anti-T-bet PE, 1:100; anti-TNF FITC, 1:100; anti-TNF PE, 1:100; anti-TOX PE, 1:100. D^bGP33-41 and D^bGP276-286 tetramers were prepared in house and were used to detect LCMV-specific $CD8^+$ T cells (dilution, 1:100). Streptavidin–PE or streptavidin–APC was purchased from Thermo Fisher Scientific. Dead cells were excluded by using Live/Dead Fixable Near-IR (dilution, 1:250) or the Yellow Dead Cell Stain Kit (dilution, 1:250) (Thermo Fisher Scientific). For cell-surface staining, antibodies were added to cells at dilutions of 1:20–1:500 in PBS supplemented with 2% FBS and 0.1% sodium azide for 30 min on ice. Cells were washed three times, fixed with fixation/permeabilization solution (BD Biosciences). For detecting cytokine production, 1×10^6 spleen cells were stimulated with pool of nine LCMV-specific peptides (GP33-41, GP70-77, GP92-101, GP118-125, GP276-286, NP166-175, NP205-212, NP235-249 and NP396-404; 200 ng ml^{-1} each) in a 96-well round-bottom plate for 5 h at 37 °C in a CO_2 incubator in the presence of GolgiPlug (BD Biosciences). To detect degranulation, splenocytes were stimulated with pool of nine LCMV-specific peptides for 5 h in the presence of GolgiPlug, GolgiStop (BD Biosciences) and anti-CD107a Alexa Fluor 488 (dilution, 1:200) (Thermo Fisher Scientific). For examining the responsiveness of LCMV-specific $CD8^+$ T cells to inflammatory cytokines, 1×10^6 splenocytes were cultured with recombinant mouse IL-12 and IL-18 (both were from R&D systems, 20 ng ml^{-1} each) for 5 h, and GolgiPlug was added, followed by culturing for 1 h. Intracellular staining was performed using the BD Cytofix/Cytoperm protocol. For detecting intranuclear proteins, the FOXP3 staining buffer set (Thermo Fisher Scientific) was used according to the manufacturer's instructions. To detect LCMV-specific $CD4^+$ T cells, splenocytes were stained with I-A^bGP66-77 tetramer (DIYKGVYQFKSV; NIH Tetramer Core Facility, Emory University) at 37 °C for 2 h (dilution, 1:200), followed by cell-surface staining as described. The samples were acquired on the Canto II, LSR II or FACSymphony A3 (BD Biosciences) system, and data were analysed using FlowJo (v.9.9.6 or 10.8.1, BD Biosciences).

Chemotaxis assay

Chemokine dilutions of PBS with CXCL9 or CXCL10 (both from R&D Systems, 0.5 μg ml^{-1}) were added to the bottom well of a 96-well Transwell plate with a 5 μm pore size (Corning). Sorted PD-1^+CD8^+ T cells ($2–3 \times 10^4$ cells in 100 μl) from LCMV chronically infected mice treated for 2 weeks were added on the top of the membrane with duplicates and allowed to migrate at 37 °C for 3 h. Numbers of migrated cells to the bottom wells were counted by Canto II (BD Biosciences). The chemotactic index was calculated as the ratio of cell numbers in the bottom well in the presence versus in the absence of chemokines.

Cell sorting

Cell sorting was performed using the FACS Aria II (BD Biosciences) system. For RNA-seq, scRNA-seq (10x Genomics) and ATAC-seq analysis, LCMV chronically infected mice (>day 40 after infection) were untreated or treated with various therapeutic modalities for 2 weeks, and D^bGP33$^+CD8^+$ T cells in spleens were sorted from pooled spleens ($n = 1–18$). Before the sort, D^bGP33$^+CD8^+$ T cells were enriched by staining the D^bGP33-APC tetramer, labelling them with anti-APC MicroBeads (Miltenyi Biotec), followed by magnetic separation using the LS column (Miltenyi Biotec). Naive ($CD44^{low}$) $CD8^+$ T cells were sorted from pooled spleens from uninfected mice ($n = 2$). For the chemotaxis assay, mice chronically infected with LCMV were treated with PD-1 monotherapy, IL-2 alone or combination therapy for 2 weeks. Cells were isolated from the spleens of each treatment group ($n = 1–8$). $CD8^+$

T cells were enriched using the CD8$^+$ T cell isolation kit (Miltenyi Biotec), followed by magnetic separation using the LS column (Miltenyi Biotec), and PD-1$^+$CD8$^+$ T cells were sorted. For experiments of adoptive transfer of two CD8$^+$ T cell subsets, splenocytes were isolated from LCMV chronically infected mice (n = 20–53), and 5×10^4 to 1×10^5 of two (PD-1$^+$CXCR5$^+$TIM3$^-$ and PD-1$^+$CXCR5$^-$TIM3$^+$) CD8$^+$ T cell subsets were sorted. The purities of the sorted cells were more than 95%.

PD-1 therapy, IL-2 and the combination therapy in vivo

PD-1 therapy, IL-2 and PD-1 + IL-2 combination therapy were performed as described previously[1]. For PD-1 monotherapy, 200 μg of rat anti-mouse PD-L1 antibody (10F.9G2, prepared in house) or rat IgG2b isotype control (LTF-2, BioXCell) was administered i.p. into LCMV chronically infected mice every 3 days for 2 weeks. For IL-2 therapy, 15,000 IU of recombinant human IL-2 (Amgen) diluted in PBS with 0.1% normal mouse serum was given i.p. twice daily for 2 weeks. For examining the requirement of PD-1 blockade for improving viral control during IL-2 therapy, 500 μg of rat anti-mouse PD-L1 antibody was administered at day 10 and 12 after starting IL-2 treatment.

PD-1 + IL-2(WT) or PD-1 + IL-2(V) combination therapy in vivo

For comparing IL-2(WT) and IL-2(V) combination therapies, recombinant human IL-2(WT) or IL-2(V), and anti-mouse PD-L1 antibodies with DAPG mutation were produced and provided by Roche as previously described[37]. For PD-1 monotherapy, 200 μg of anti-mouse PD-L1 antibody (Roche) or mouse IgG1 isotype control (MOPC-21, BioXCell) was administered into LCMV chronically infected mice every 3 days for 2 weeks. For the combination therapy, IL-2(WT) or IL-2(V) therapy was combined with PD-1 therapy, where 1 μg of IL-2(WT) (Roche) or 10 μg of IL-2(V) (Roche) diluted in PBS with 0.1% normal mouse serum was given i.p. twice daily for 2 weeks. In the chronic infection model with LCMV-specific CD4$^+$ T cells, IL-2(WT) and IL-2(V) was given i.p. once daily from day 25 to day 33 after the mice were infected with LCMV clone 13.

CD8$^+$ T cell depletion

For depleting CD8$^+$ T cells during PD-1 + IL-2 combination therapy, 200 μg of rat anti-mouse CD8 antibody (2.43, BioXCell) or rat IgG2b isotype control (LTF-2, BioXCell) was administered i.p. into LCMV chronically infected mice every 3 days for 2 weeks.

CD25 blockade

For examining whether CD25 engagement by IL-2 was essential for the therapeutic efficacy of PD-1 + IL-2 combination therapy, 200 μg of rat-mouse chimeric antibody PC61-mIgG1 (N297Q) (Biogen)[36] or mouse IgG1 isotype control (MOPC-21, BioXCell) was administered i.p. into LCMV chronically infected mice every 3 days for 2 weeks of PD-1 + IL-2 combination therapy.

Adoptive transfer of two CD8$^+$ T cell subsets

A total of 5×10^4 to 1×10^5 of two (PD-1$^+$CXCR5$^+$TIM3$^-$ and PD-1$^+$CXCR5$^-$TIM3$^+$) CD8$^+$ T cell subsets isolated from LCMV chronically infected mice (CD45.2) were transferred into infection-matched recipient mice (CD45.1). Groups of these mice were then either left untreated, or given anti-PD-L1 antibodies, IL-2 therapy or the combination therapy for 2 weeks.

Histological assessment

Sections (4–5 μm) of formalin-fixed paraffin-embedded (FFPE) liver samples were stained with haematoxylin and eosin (H&E) or processed for TUNEL analysis. The slides were scanned using the Leica Aperio GT 450 slide scanner and reviewed by a gastrointestinal and liver pathologist. Portal inflammation was scored on a four-point scale (0–3) as minimal to no inflammation (0); mild (1); moderate (2); and severe (3). Lobular inflammation was scored on a four-point scale in two subcategories: immune cell clusters (none (0); up to 1 per 1 mm^2 field (1); up to 2 per 1 mm^2 field (2); and 3 or more clusters per a one mm^2 field (3)) and overall degree of lobular inflammation including sinusoidal infiltration of lymphocytes and degree of hepatocyte injury (no or rare lobular inflammation (0); mild inflammation (1); moderate (2); and severe (3)). The overall lobular inflammation was scored on a seven-point scale (0–6). The maximal number of acidophil bodies in a 1 mm^2 area was quantified and scored on a four-point scale (0–3) as follows: no acidophil bodies (0); one to two acidophil bodies (1); three to four bodies (2); and five or more acidophil bodies (3). For the TUNEL assay, five 1 mm^2 (five ×200 fields) hotspots of positive sinusoidal cell or hepatocyte staining per tissue were counted. The images were processed using QuPath[42].

Measurement of serum ALT levels

Serum samples pooled from 2–3 mice were sent to the Comparative Pathology Laboratory at University of Georgia and ALT levels were measured with a Roche Cobas c501 biochemical analyser.

RNA-seq

For the comparison of untreated, PD-1 therapy, IL-2 treatment and combination therapy, total RNA was isolated using the Direct-zol RNA Miniprep kit (Zymo Research), with on-column DNase digestion. RNA-seq libraries were prepared using 150 ng of total RNA and the KAPA Stranded mRNA-seq Kit (Kapa Biosystems). Each library was indexed using barcoded primers (BIOO Scientific) and was amplified for 10 cycles. Then, 200 bp to 350 bp fragments of barcoded PCR products were separated by 2% E-Gels (Thermo Fisher Scientific) and purified using the Gel DNA Purification Kit (Zymo Research). The final PCR products were sequenced on the Illumina HiSeq 2500 platform. For comparing IL-2(WT) combination versus IL-2(V) combination therapy, total RNA from samples was isolated using Trizol (Thermo Fisher Scientific) and the RNeasy Micro kit (Qiagen) according to the manufacture's protocols at Emory Integrated Genomics Core. Preparation of a standard RNA-seq library was performed at Hudson Alpha. In brief, RNA amplification was performed using the Nugen Ovation RNAseq v2 kit. Amplified cDNA was normalized and sonicated on the Covaris LE200 using a protocol designed to achieve a target insert size of 350 bp. The samples were prepared using the KAPA Hyper Prep kit and GSL v5.8 indexes. Pooled libraries were sequenced on the Illumina NovaSeq 6000 system with 100 bp paired-end reads.

Reads were mapped to the GRCm38/mm10 genome[43] using HISAT2 (v.2.1.0)[44]. Gene expression was quantified using featureCounts[45]. DESeq2[46] was used to normalize for library size and calculate differential expression across groups. A gene was considered to be differentially expressed across the treatment groups with an adjusted P value of <0.05 with an average expression of >20 normalized counts across all samples. Principal component analysis was performed on all detected genes using the regularized log transformation from DESeq2. GSEA[47] was performed against canonical CD8$^+$ T cell gene sets, generated by using a previously published data (Gene Expression Omnibus (GEO): GSE9650; and NCBI BioProject: PRJNA412602)[16,17]. The exhaustion signature was defined as genes that were at least twofold upregulated in D^{b}GP33$^+$CD8$^+$ T cells isolated from chronically mice infected with LCMV clone 13 compared to D^{b}GP33$^+$CD8$^+$ T cells isolated from mice 8 days after acute LCMV Armstrong infection. The effector signature was generated by taking the top 400 most upregulated genes between naive CD8$^+$ T cells and D^{b}GP33$^+$CD8$^+$ T cells isolated from mice 8 days after acute LCMV Armstrong infection[16]. The memory signature was generated by upregulated genes between naive CD8$^+$ T cells and LCMV-specific CD8$^+$ T cells isolated from mice 48 days after acute LCMV Armstrong infection[17]. GSEA was performed using $\log_2$-transformed fold change difference between classes. To determine the relative enrichment of these signatures in each treatment group, GSEA comparing the designated treatment regimen to the other three datasets was performed.

RNA-seq data were visualized using Microsoft Excel (v.14.4.3), Prism (v.9.3.1, GraphPad) and the ggplot2 R package[48].

scRNA-seq

scRNA-seq libraries were generated using the Chromium Single Cell 5′ Library & Gel Bead Kit (10x Genomics) according to the manufacturer's protocol. In brief, $D^bGP33^+CD8^+$ T cells or naive $CD44^{low}$ $CD8^+$ T cells were sorted and captured into the gel beads-in-emulsion. After reverse transcription, the gel beads-in-emulsion were disrupted and the barcoded cDNA was isolated, pooled and amplified by PCR (13 cycles). The amplified cDNA was fragmented, and processed for end repair and A-tailing followed by a sample index PCR (16 cycles). The purified libraries were sequenced to a depth of 50,000 reads per cell on the HiSeq 3000 (Illumina) system with 26 cycles for read 1, 8 cycles for index 1 (i7) and 91 cycles for read 2.

Alignment, filtering, barcode counting and unique molecular identifier counting were performed using Cell Ranger v.3.1. Data were further analysed using Seurat (v.3.0)[49]. In brief, cells with a percentage of mitochondrial genes below 0.05% were included. Cells with more than 4,000 or less than 1,000 detected genes were considered to be outliers and were excluded from the downstream analyses. Raw unique molecular identifier counts were normalized to unique molecular identifier count per million total counts and log-transformed. Variable genes were selected on the basis of average expression and dispersion. PCA was performed using variable genes. Clusters were identified using the shared nearest neighbour algorithm in Seurat and *t*-SNE plots were generated based on selected PCA dimensions. Marker genes were identified using the Seurat function FindAllMarkers. log-normalized data are shown in the form of feature plots with the scale in a range of 0 (grey) to 2.5–5 (purple). Gene set scoring was performed using the VISION R package (v.1.1.0). The scoring algorithm was described previously[50]. In brief, expression of signature genes is weighted on the basis of predicted dropout probability calculated from nearest neighbours, and the normalized expression summed for all of the genes in the gene set. The gene sets used were the same as in RNA-seq.

Analysis of multiparameter conventional flow cytometry

For examining phenotypes of LCMV-specific $CD8^+$ T cells, conventional 19-colour flow cytometry data of $D^bGP33^+CD8^+$ T cells after different treatments were concatenated, and processed for UMAP plugins (nearest neighbours = 15, minimum distance = −0.5 and number of components = 2)[51] and the FlowSOM clustering algorithm (number of meta clusters = 3)[52] using the parameters of TCF1 Alexa Fluor 488, granzyme B BV421, TIM3 BUV395, CX3CR1 BV785, CD101 PE-Cy7, CD218a PE, CXCR5 PE-Dazzle, SLAMF6 BUV737, CD73 BV605, CXCR3 BV480, Ly-6C R700 and CD44 BUV805 in FlowJo v.10.8.1 (BD Biosciences).

To determine which $CD8^+$ T cells in three clusters produced effector cytokines or degranulated after stimulation with LCMV-specific peptides, 14-colour flow cytometry data of PD-1^+CD8^+ T cells were concatenated and used for the subsequent analysis as described above using the parameters of TCF1 Alexa Fluor 488 (or PE), granzyme B BV421, CX3CR1 BV785, CD101 APC, CD218a PerCP-eFluor710 (or PE), TIM3 BUV395, SLAMF6 BUV737 and CD44 BUV805. The distribution of $IFN\gamma^+$, $IFN\gamma^+TNF\alpha^+$, $IFN\gamma^+IL\text{-}2^+$ and $IFN\gamma^+CD107a^+$ cells was checked in the defined three clusters. TCF1 was excluded from the staining panel when intracellular IL-2 staining was performed by BD Cytofix/Cytoperm protocol due to the incompatibility of PE anti-IL-2 (JES6-SH4, BD Biosciences) for the FOXP3 staining buffer protocol.

For testing which $CD8^+$ T cells in three clusters produced IFNγ in response to IL-12 + IL-18 stimulation, $D^bGP33^+CD8^+$ T cells from mice treated with various regimens were concatenated and processed for the subsequent analysis as described above using parameters of TCF1 Alexa Fluor 488, granzyme B BV421, CX3CR1 BV785, CD101 PE-Cy7, CD218a PE, TIM3 BUV395, SLAMF6 BUV737 and CD44 BUV805. $IFN\gamma^+$ cells were identified in the defined three clusters.

ATAC-seq

ATAC-seq analysis was performed as described elsewhere[53]. In brief, $3–5 \times 10^4$ sorted cells were washed with cold PBS, then with RSB buffer (10 mM Tris-HCL pH 7.4, 10 mM NaCl, 3 mM $MgCl_2$) and lysed with lysis buffer (RSB buffer + 0.1% IGEPAL CA-630 + 0.1% Tween-20). Lysed nuclei were resuspended in the transposase reaction mix (25 µl 2× TD buffer, 1 µl Illumina transposase and 24 µl nuclease-free water) and incubated at 37 °C for 30 min. DNA from the transposase reaction was purified using the MinElute PCR purification Kit (Qiagen). PCR amplification was performed using Nextera PCR primers. The final libraries were quantified using the KAPA Library Quantification Kit and sequenced on the Illumina HiSeq 2500 system by ELIM Biopharm. Reads were aligned to mm10 using bowtie2, discarding read pairs with a mapping quality of less than 20. Peaks were called separately for each sample using MACS2. A consensus peak set was derived by combining peaks from all of the samples and subsequently merging peaks that overlapped >50%. Peaks that overlapped with regions identified in the ENCODE blacklist[54] were removed from the analysis. Peaks were visualized using IGV, with the *y* axis set at the scale of reads per base pair normalized to the total number of reads assigned in consensus peaks for each sample. Gene and TSS annotations were based on the RefSeq database. The ability of the peaks to discriminate between subpopulations was assessed by selecting 5,000 peaks with the greatest overall variance after a variance stabilizing transformation. PCA was performed on the same data and a previously published dataset (PRJNA546023)[30]. To assess differential openness, we used conditional quantile normalization[55] followed by limma voom with quality weights[56] on the matrix of insertions in peaks by sample. A linear model was fit to the data, and then contrasts for binary comparisons among the sample groups were set up. Peaks were considered to be differentially open if the robust empirical Bayes *P* value for a contrast from the fitted linear model was less than 0.05 after multiple-hypothesis correction using the Benjamini–Hochberg procedure. To determine which regulatory elements contributed mostly towards alterations, each *k*-means cluster was examined for enrichment of transcription-factor-binding motifs using Homer[57].

Statistical analysis

Prism (v.9.3.1, GraphPad) was used for statistical analysis. The difference among the experimental groups was assessed using two-tailed unpaired *t*-tests or two-tailed unpaired Mann–Whitney *U*-tests for comparing two groups. One-way ANOVA with Tukey's multiple-comparison test or Kruskal–Wallis test with Dunn's multiple-comparison test was used for comparing more than two groups.

Reporting summary

Further information on research design is available in the Nature Research Reporting Summary linked to this article.

Data availability

All processed RNA-seq, scRNA-seq and ATAC-seq data supporting the findings of this study have been deposited at GEO under accession code GSE206739. Previously published Affymetrix microarrays (GEO: GSE9650)[16], RNA-seq (NCBI BioProject: PRJNA412602)[17] and ATAC-seq data (NCBI BioProject: PRJNA546023)[30] are included for the analysis in this study. Source data are provided with this paper.

Code availability

Custom code for RNA-seq, scRNA-seq and ATAC-seq data analysis are available from the corresponding author on reasonable request.

41. Wherry, E. J., Blattman, J. N., Murali-Krishna, K., van der Most, R. & Ahmed, R. Viral persistence alters CD8 T-cell immunodominance and tissue distribution and results in distinct stages of functional impairment. *J. Virol.* **77**, 4911–4927 (2003).
42. Bankhead, P. et al. QuPath: open source software for digital pathology image analysis. *Sci. Rep.* **7**, 16878 (2017).
43. Zerbino, D. R. et al. Ensembl 2018. *Nucleic Acids Res.* **46**, D754–D761 (2018).
44. Kim, D., Langmead, B. & Salzberg, S. L. HISAT: a fast spliced aligner with low memory requirements. *Nat. Methods* **12**, 357–360 (2015).
45. Liao, Y., Smyth, G. K. & Shi, W. featureCounts: an efficient general purpose program for assigning sequence reads to genomic features. *Bioinformatics* **30**, 923–930 (2014).
46. Love, M. I., Huber, W. & Anders, S. Moderated estimation of fold change and dispersion for RNA-seq data with DESeq2. *Genome Biol.* **15**, 550 (2014).
47. Subramanian, A. et al. Gene set enrichment analysis: a knowledge-based approach for interpreting genome-wide expression profiles. *Proc. Natl Acad. Sci. USA* **102**, 15545–15550 (2005).
48. Hadley, W. *ggplot2: Elegant Graphics for Data Analysis* (Springer, 2016).
49. Satija, R., Farrell, J. A., Gennert, D., Schier, A. F. & Regev, A. Spatial reconstruction of single-cell gene expression data. *Nat. Biotechnol.* **33**, 495–502 (2015).
50. DeTomaso, D. & Yosef, N. FastProject: a tool for low-dimensional analysis of single-cell RNA-Seq data. *BMC Bioinform.* **17**, 315 (2016).
51. McInnes, L., Healy, J., Saul, N. & Großberger, L. UMAP: uniform manifold approximation and projection. *J. Open Source Softw.* **3**, 861 (2018).
52. Van Gassen, S. et al. FlowSOM: using self-organizing maps for visualization and interpretation of cytometry data. *Cytometry A* **87**, 636–645 (2015).
53. Buenrostro, J. D., Wu, B., Chang, H. Y. & Greenleaf, W. J. ATAC-seq: a method for assaying chromatin accessibility genome-wide. *Curr. Protoc. Mol. Biol.* **109**, 21.29.1–21.29.9 (2015).
54. Amemiya, H. M., Kundaje, A. & Boyle, A. P. The ENCODE Blacklist: identification of problematic regions of the genome. *Sci. Rep.* **9**, 9354 (2019).
55. Hansen, K. D., Irizarry, R. A. & Wu, Z. Removing technical variability in RNA-seq data using conditional quantile normalization. *Biostatistics* **13**, 204–216 (2012).
56. Liu, R. et al. Why weight? Modelling sample and observational level variability improves power in RNA-seq analyses. *Nucleic Acids Res.* **43**, e97 (2015).
57. Heinz, S. et al. Simple combinations of lineage-determining transcription factors prime *cis*-regulatory elements required for macrophage and B cell identities. *Mol. Cell* **38**, 576–589 (2010).

Acknowledgements This work was supported by National Institutes of Health (NIH) grants R01AI030048 (to R.A.), P01AI056299 (to R.A., G.J.F. and A.H.S.), P50CA101942 (to G.J.F. and A.H.S.), P01CA236749 (to G.J.F. and A.H.S.), R01AI129191 (to J.J.G.), P50CA217691 (to S.S.R. and R.A.), and the Roche pRED ROADS programme (ROADS grant 55440 funded by Roche, ID ROADS-034; to R.A.). We thank staff at the Emory University School of Medicine Flow Cytometry Core (K. Fife and R. Karaffa), Yerkes Nonhuman Primate Genomics Core (K. Pellegrini and S. Bosinger; NIH P51OD011132), Emory Integrated Genomics Core (EIGC) Shared Resource of Winship Cancer Institute of Emory University and NIH/NCI (L. Griffiths; 2P30CA138292-04), Cancer Tissue and Pathology Shared Resource Facility of the Winship Cancer Institute of Emory University and NIH/NCI (P30CA138292), and the Mouse Histology and Phenotyping Lab at the Northwestern University Robert H. Lurie Comprehensive Cancer Center and NIH/NCI (P30CA060553). W.H.H. is supported by NIH grant K99AI153736 and a Cancer Research Institute Irvington Postdoctoral Fellowship. S.J.I. is supported by National Research Foundation of Korea (NRF) grant 2020R1F1A1075668 funded by the Korean government (MSIT). The content is solely the responsibility of the authors and does not necessarily represent the official views of the National Institutes of Health.

Author contributions M.H., K.A. and R.A. designed experiments. M.H., K.A., R.C.O., A.W., Judong Lee, D.T.M., C.D.S, S.S.R., W.J.G., J.J.G., W.J.L. and R.A. analysed the experiments. M.H., R.C.O., A.W., Judong Lee, D.T.M., J.L.R, C.D.S., S.J.I., Junghwa Lee, J.-X.L., B.H. and E.E.W. performed experiments. M.H., P.L., H.T.K. and W.H.H. analysed RNA-seq data. M.A.C., H.T.K. and D.J.M. analysed scRNA-seq data. R.R.J., W.J.G. and J.J.G. analysed ATAC-seq data. G.J.F., A.H.S., A.P., V.T., C.K., P.U. and K.A.S. contributed materials. M.H. and R.A. wrote the manuscript. All of the authors contributed to writing the manuscript and provided feedback.

Competing interests R.A. has patents related to PD-1 pathway (8,652,465 and 9,457,080) licensed to Roche. A.H.S has patents and pending royalties from Roche and Novartis on intellectual property on the PD-1 pathway (patent 7,432,059 with royalties paid from Roche, Merck, Bristol Myers Squibb, EMD-Serono, Boehringer-Ingelheim, AstraZeneca, Leica, Mayo Clinic, Dako and Novartis; patent 7,722,868 with royalties paid from Roche, Merck, Bristol Myers Squibb, EMD-Serono, Boehringer-Ingelheim, AstraZeneca, Leica, Mayo Clinic, Dako and Novartis; patents 8,652,465 and 9,457,080 licensed to Roche; patents 9,683,048, 9,815,898, 9,845,356, 10,202,454 and 10,457,733 licensed to Novartis; and patents 9,580,684, 9,988,452 and 10,370,446 issued to none). G.J.F. has patents and pending royalties on the PD-1–PD-L1 pathway from Roche, Merck MSD, Bristol Myers Squibb, Merck KGaA, Boehringer-Ingelheim, AstraZeneca, Dako, Leica, Mayo Clinic and Novartis (see Supplementary Data 4). G.J.F. has served on advisory boards for Roche, Bristol Myers Squibb, Xios, Origimed, Triursus, iTeos, NextPoint, IgM, Jubilant, Trillium, GV20 and Geode. G.J.F. has equity in Nextpoint, Triursus, Xios, iTeos, IgM, GV20 and Geode. V.T., C.K. and P.U. are employed by Roche with stock options. C.K. and P.U have a patent application with Roche: WO2012107417. The other authors declare no competing interests.

Additional information

Supplementary information The online version contains supplementary material available at https://doi.org/10.1038/s41586-022-05257-0.

Correspondence and requests for materials should be addressed to Rafi Ahmed.

Peer review information *Nature* thanks Stephen Jameson and the other, anonymous, reviewer(s) for their contribution to the peer review of this work.

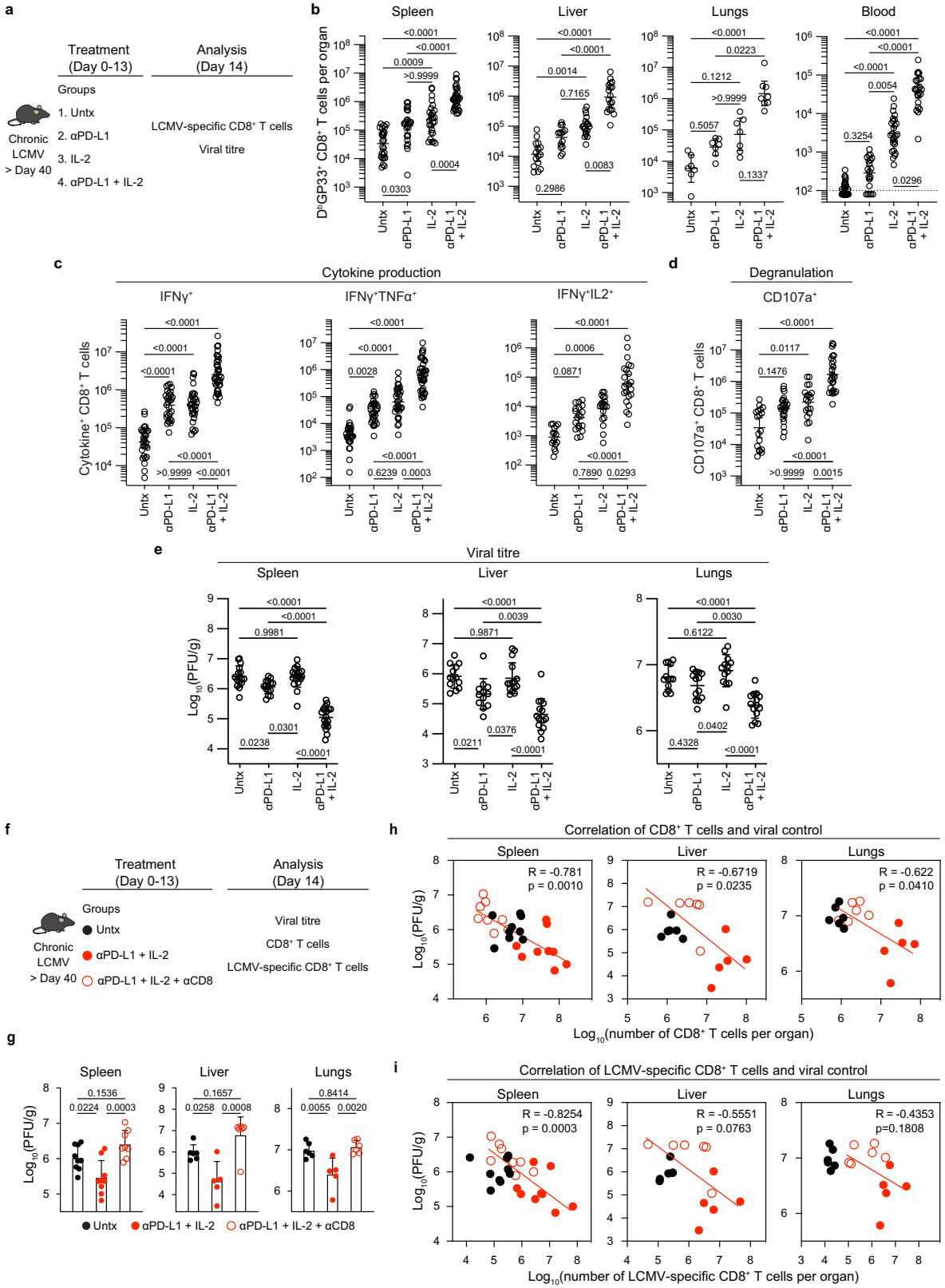

Extended Data Fig. 1 | See next page for caption.

Extended Data Fig. 1 | PD-1 + IL-2 combination therapy synergistically expands functional LCMV-specific CD8$^+$ T cells that mediate viral control during chronic infection. a, Experimental setup for panels **b**–**e**. Mice chronically infected with LCMV were either left untreated, or treated with anti-PD-L1 antibody alone (200 µg i.p., every 3 days), IL-2 therapy alone (15,000 IU i.p., twice daily), or the combination therapy for 2 weeks. **b**, Numbers of D^bGP33^+ $CD8^+$ T cells in the indicated tissues and blood (per 1×10^6 PBMCs). **c**, **d**, Spleen cells were stimulated with pools of LCMV-specific peptides for 5 h and analysed by intracellular staining of cytokines (**c**) and degranulation (**d**). **e**, Viral titre in the indicated tissues. **f**, Experimental setup for panels **g**–**i**. LCMV chronically infected mice were either left untreated, or treated with combination therapy, or combination therapy plus anti-CD8 depleting antibody (200 µg i.p., every 3 days) for 2 weeks. **g**, Viral titre in the indicated tissues of the three groups of mice. **h**, **i**, Correlation between viral titre in the various tissues and the number of $CD8^+$ T cells (**h**), or LCMV-specific (D^bGP33^+ and D^bGP276^+) $CD8^+$ T cells (**i**). Results were pooled from 3-13 experiments (**b**–**e**) with n = 25-32 (spleen), n = 14-18 (liver), n = 7-8 (lung), and n = 20-33 (blood) (**b**), with n = 28-38 ($IFN\gamma^+$), n = 28-38 ($IFN\gamma^+TNF\alpha^+$), n = 16-23 ($IFN\gamma^+IL\text{-}2^+$), and n = 18-25 ($CD107a^+$) (**c**), and with n = 16-19 (spleen), n = 12-15 (liver), and n = 13-14 (lung) (**e**) per group or pooled from 2-3 experiments with 2-4 mice per group in each experiment (**g**–**i**). Data are presented as geometric mean and 95% CI (**b**–**d**), mean and SD (**e**, **g**), or linear regression line and Pearson correlation coefficient (two-tailed) (**h**, **i**) with p values. Statistical comparisons were performed using Kruskal-Wallis test with Dunn's multiple-comparison test (**b**–**d**) or one-way ANOVA with Tukey's multiple-comparison test (**e**). Untx, untreated.

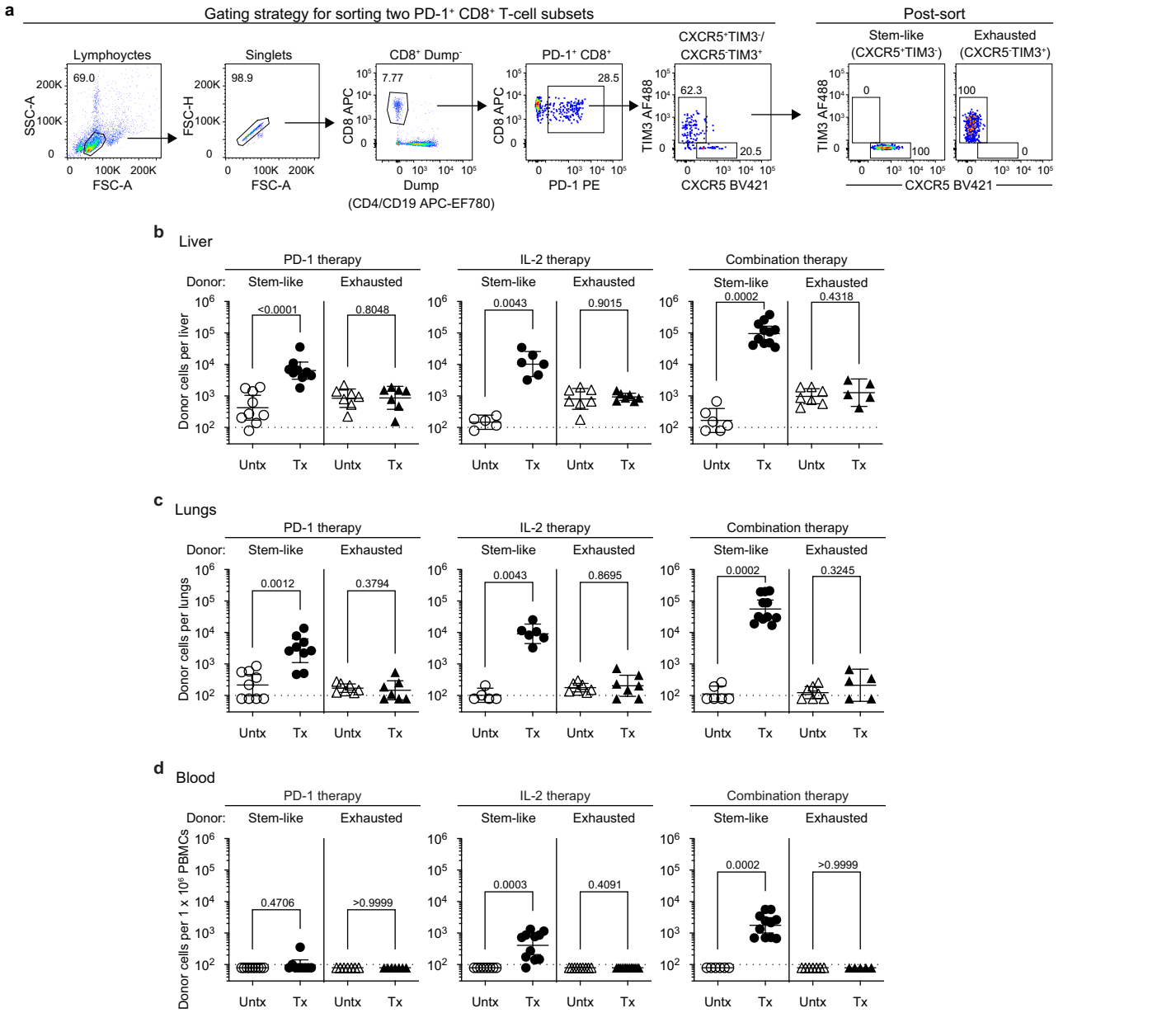

Extended Data Fig. 2 | The proliferative response after PD-1 blockade, IL-2 therapy, and PD-1 + IL-2 combination therapy comes from the same population of PD-1$^+$ TCF1$^+$ stem-like CD8$^+$ T cells. a, Gating strategy for sorting stem-like (PD-1$^+$CXCR5$^+$TIM3$^-$) and exhausted (PD-1$^+$CXCR5$^-$TIM3$^+$) CD8$^+$ T-cell subsets isolated from spleens of CD45.2$^+$ LCMV chronically infected mice. **b**–**d**, Summary data for the numbers of donor CD45.2$^+$ CD8$^+$ T cells after 2 weeks of PD-1 therapy, IL-2 therapy, and the combination therapy in liver (**b**), lungs (**c**), and blood (per 1 x 10^6 PBMCs) (**d**) of the recipient mice. Results were pooled from 3-4 experiments with n = 7-9 (PD-1 therapy), n = 5-13 (IL-2 therapy), and n = 5-11 (PD-1 + IL-2 combination therapy) per group. Data are presented as geometric mean and 95% CI (**b**–**d**) with p values. Dotted line indicates the limit of detection. Statistical comparisons were performed by using two-tailed unpaired Mann-Whitney test. AF, Alexa Fluor; EF, eFluor; Tx, treated; Untx, untreated.

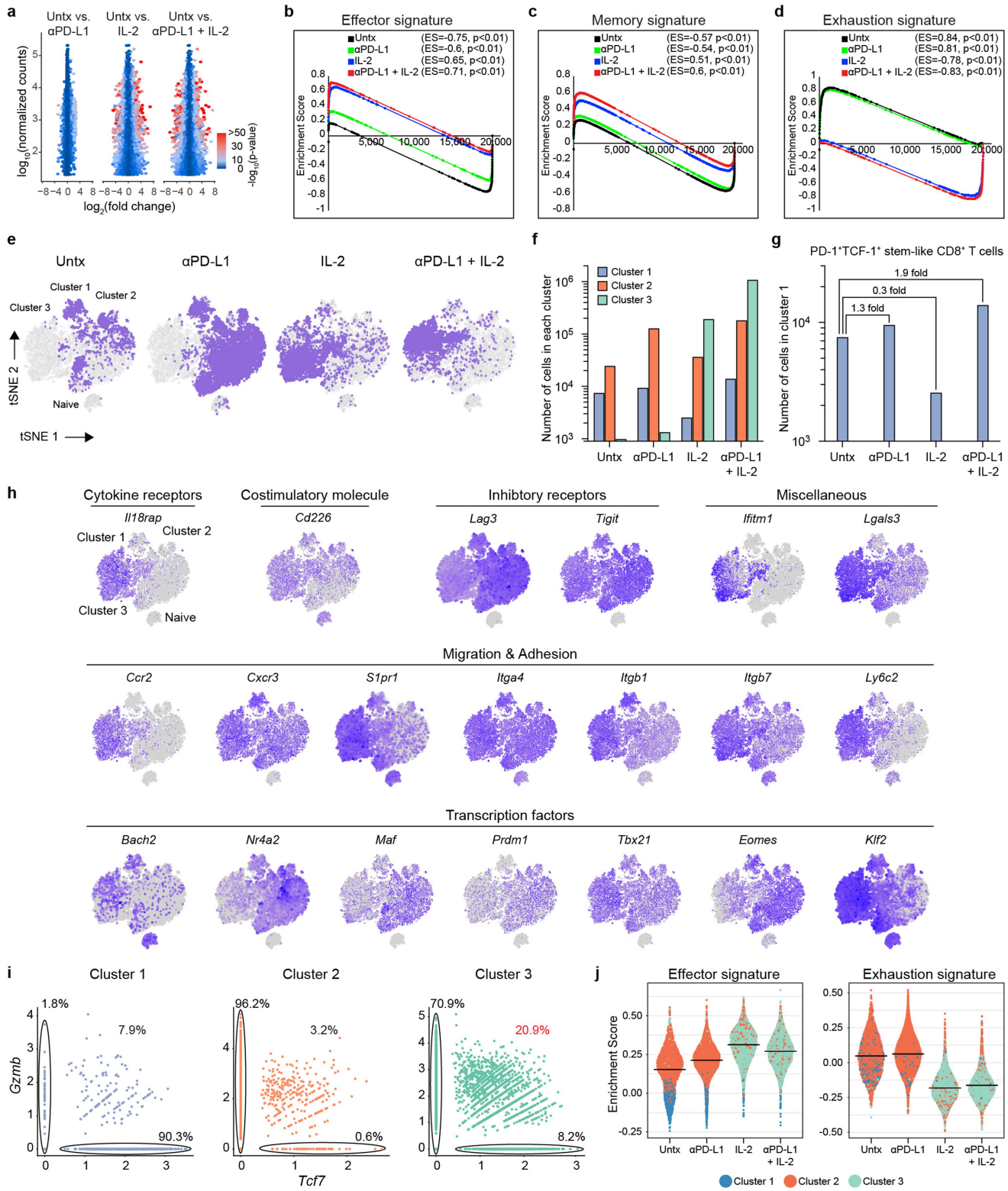

Extended Data Fig. 3 | See next page for caption.

Extended Data Fig. 3 | Transcriptional profiling of LCMV-specific CD8$^+$ T cells generated by PD-1 monotherapy, IL-2 treatment, and PD-1 + IL-2 combination therapy during chronic infection. Mice chronically infected with LCMV were treated with PD-1 monotherapy, IL-2 alone, or combination therapy for 2 weeks. LCMV-specific D^{b}GP33$^+$ CD8$^+$ T cells from spleens of each treatment group were sorted for RNA-seq (**a**–**d**) and scRNA-seq (**e**–**j**). As a control, naive (CD44^{lo}) CD8$^+$ T cells were also sorted for scRNA-seq (**e**–**j**). **a**, MA plots for gene expression of D^{b}GP33$^+$ CD8$^+$ T cells after the indicated treatments. **b**–**d**, GSEA of D^{b}GP33$^+$ CD8$^+$ T cells generated by the indicated treatments for effector signature (acute infection) (**b**), memory signature (acute infection) (**c**), and exhaustion signature (chronic infection) (**d**). **e**, The t-SNE projection of naive CD44^{lo} CD8$^+$ T cells and D^{b}GP33$^+$ CD8$^+$ T cells in 4 treatment groups during chronic infection. Naive and four treatment samples were distributed and overlaid onto the four clusters. **f**, Numbers of cells in clusters 1, 2, and 3. **g**, Numbers of cells in cluster 1. Numbers of total D^{b}GP33$^+$ CD8$^+$ T cells per spleen were estimated from geometric mean of Extended Data Fig. 1b (**f**, **g**). **h**, Normalized expression of several representative genes is shown within the 4 clusters **i**, Co-expression patterns of *Tcf7* and *Gzmb* in cells of each cluster are shown. **j**, GSEA of D^{b}GP33$^+$ CD8$^+$ T cells generated by the different treatments for effector signature (acute infection) and exhaustion signature (chronic infection). Enrichment score for the signature in four treatment samples are shown as violin plots with horizontal bars of mean. Results were pooled from 2 (**a**–**d**) and 1-2 (**e**–**j**) experiments with n = 2-18 mice per group in each experiment. ES, enrichment score; Untx, untreated.

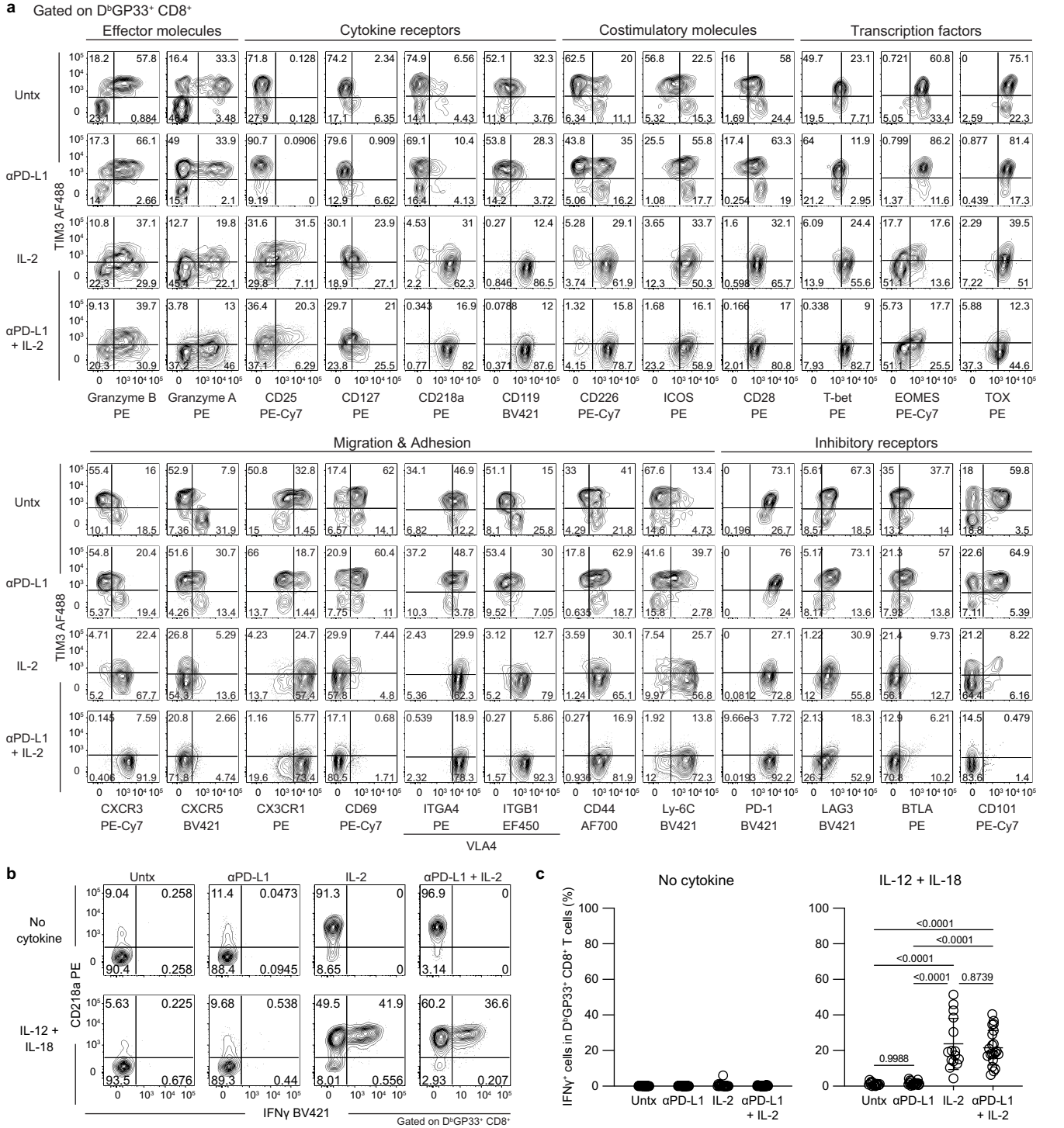

Extended Data Fig. 4 | Phenotypic and functional analysis of LCMV-specific CD8⁺ T cells generated by PD-1, IL-2, and combination therapy during chronic infection. LCMV chronically infected mice were either left untreated, or treated with anti-PD-L1 antibody alone, IL-2 therapy alone, or the combination therapy for 2 weeks. **a**, Representative FACS plots for co-expression of TIM3 and various phenotypic markers on D^bGP33^+ $CD8^+$ T cells in spleens. **b**, **c**, One million splenocytes were cultured with recombinant mouse IL-12 and IL-18 (20 ng ml^{-1} each) for 5 h, then GolgiPlug was added, followed by culturing for 1 h. Note that no viral peptides were added to the culture. Cells were stained with surface markers including D^bGP33-specific tetramer, fixed, and followed by intracellular staining of IFNγ. **b**, Representative FACS plots for co-staining of CD218a and IFNγ gated on D^bGP33^+ $CD8^+$ T cells after the indicated treatments. **c**, Summary plots for the frequency of $IFN\gamma^+$ cells in D^bGP33^+ $CD8^+$ T cells. Results shown are representative flow plots from 2-7 experiments (**a**, **b**) or pooled from 7 experiments (**c**) with n = 2-5 per group in each experiment. Data are presented as mean and SD with p values (**c**). Statistical comparisons were performed using one-way ANOVA with Tukey's multiple-comparison test (**c**). AF, Alexa Fluor; EF, eFluor; Untx, untreated.

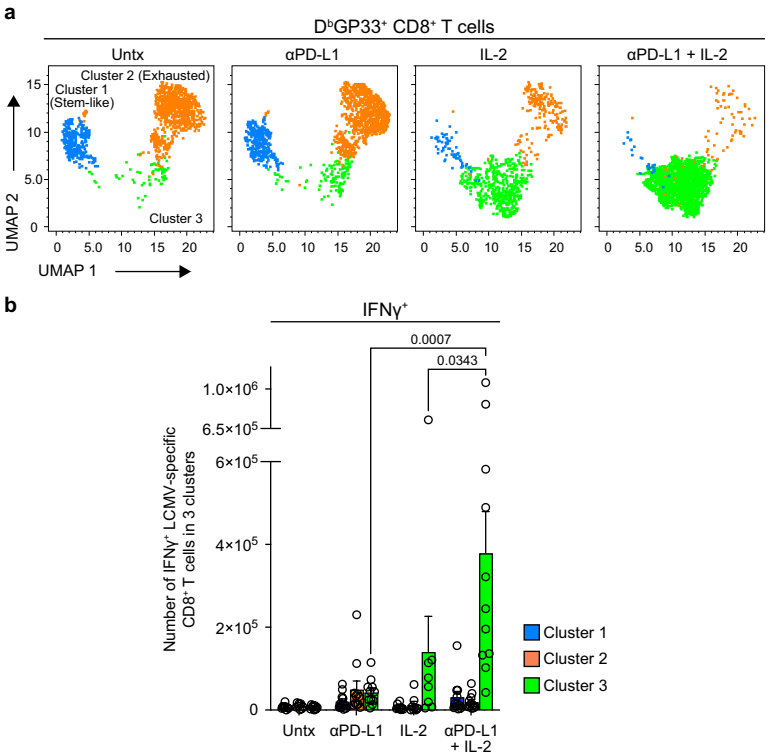

Extended Data Fig. 5 | Identification of LCMV-specific CD8$^+$ T cells generated after PD-1, IL-2, and combination therapy that produce cytokine after peptide stimulation. LCMV chronically infected mice were either left untreated, or treated with anti-PD-L1 antibody alone, IL-2 therapy alone, or the combination therapy for 2 weeks. Spleen cells were stimulated with pools of LCMV-specific peptides for 5 h and analysed by intracellular staining for cytokine production. **a**, Representative UMAP with FlowSOM overlay of D^{b}GP33$^+$ CD8$^+$ T cells isolated from spleens after the indicated treatments shows the distribution of cells in three clusters. **b**, Summary data for numbers of IFNγ$^+$ LCMV-specific CD8$^+$ T cells in the defined 3 clusters in the different treatment groups is shown. Results were pooled from 4 experiments with 2-3 mice per group in each experiment. Data are presented as mean and SEM (**b**) with p values. Statistical comparisons were performed using Kruskal-Wallis test with Dunn's multiple-comparison test (d, e). Untx, untreated.

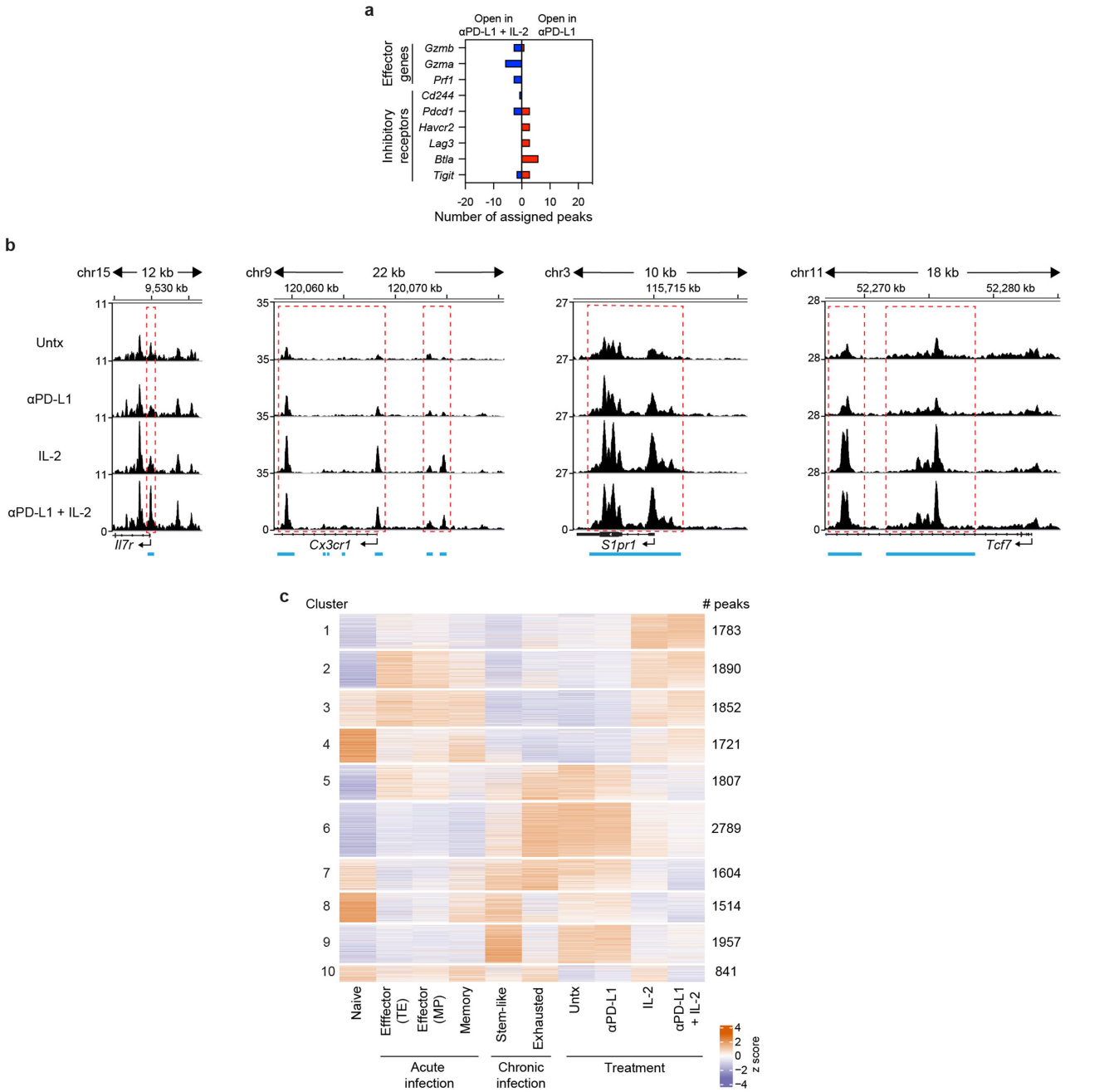

Extended Data Fig. 6 | Chromatin accessibility profiling of LCMV-specific CD8⁺ T cells in acute and chronic infection and after PD-1 treatment, IL-2 or PD-1 + IL-2 combination therapy. a, Gene annotations of differentially accessible distal regulatory regions in D^bGP33^+ $CD8^+$ T cells of mice treated with anti-PD-L1 and PD-1 + IL-2 combination therapy. The number of differentially open gene regulatory regions for genes of functional importance in D^bGP33^+ $CD8^+$ T cells after PD-1 monotherapy vs. PD-1 + IL-2 combination therapy is shown. **b**, Accessibility tracks for representative genes in LCMV-specific D^bGP33^+ $CD8^+$ T cells generated by various treatments during chronic infection. Light blue lines beneath each panel indicate differentially accessible regions in D^bGP33^+ $CD8^+$ T cells generated by PD-1 therapy versus PD-1 + IL-2 combination therapy. Red dotted lines highlight the regions indicated by the light blue lines. **c**, Heat map with 10 clusters generated by using *k*-means clustering of 16,758 DARs among D^bGP33^+ $CD8^+$ T cells generated by the combination therapy. Then, naive $CD8^+$ T cells and various LCMV-specific $CD8^+$ T-cell subsets during acute and chronic infections were incorporated into the heat map. Results were pooled from 3 experiments of ATAC-seq with n = 12-18 for untreated mice or n = 1-3 for treatment samples per group in each experiment. ATAC-seq data for naive, acute (memory precursor (MP), terminal effector (TE), and memory), and chronic (stem-like and exhausted) was from our previous study[30]. Untx, untreated.

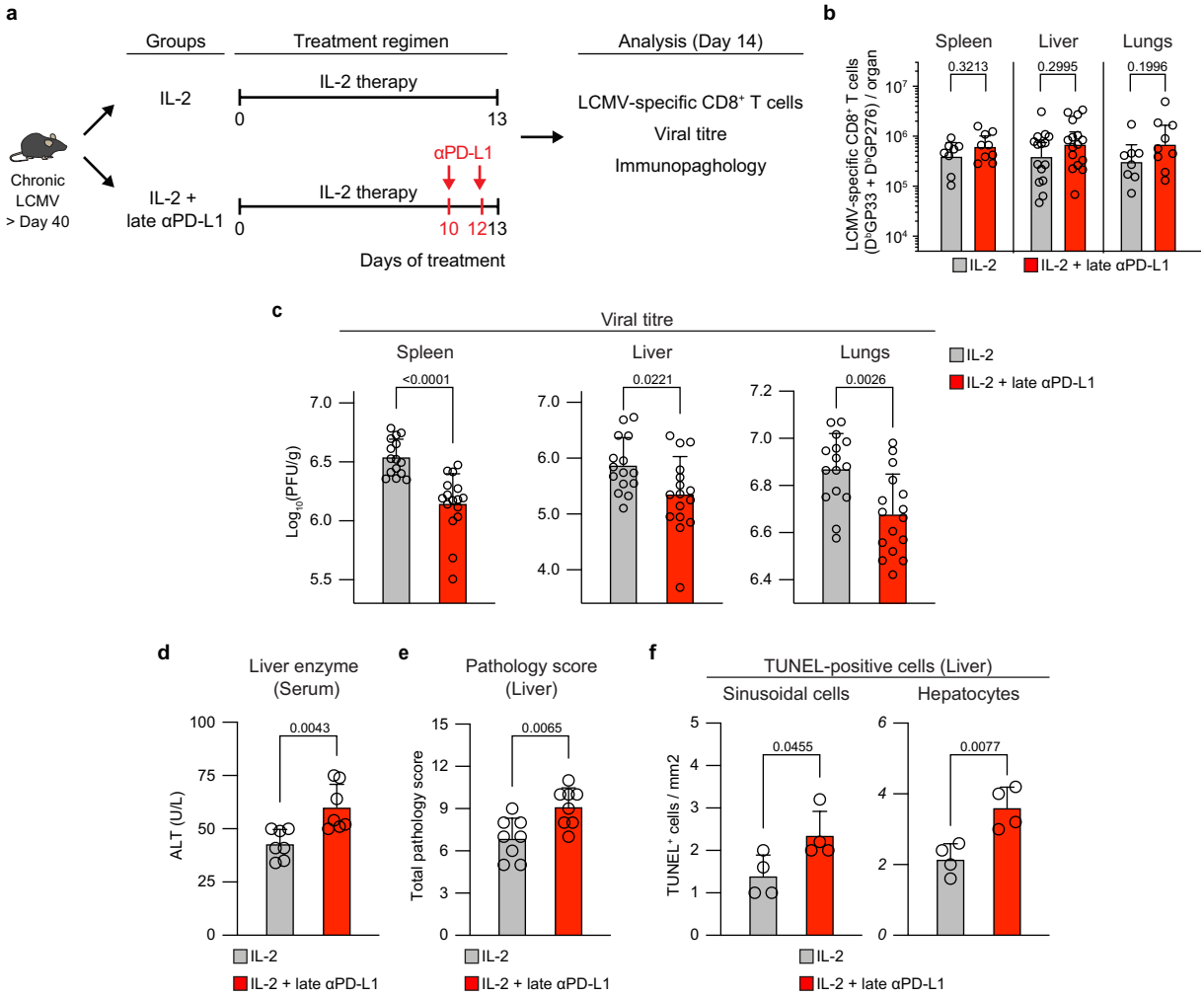

Extended Data Fig. 7 | Importance of PD-1/PD-L1 blockade at the target site in reducing viral load during chronic LCMV infection. a, Experimental design. Mice chronically infected with LCMV were divided into two groups; one group was treated with IL-2 only for 13 days (IL-2 group), and the second group was given IL-2 for 10 days followed by 2 doses of anti-PD-L1 antibody on days 10 and 12 (IL-2 + late anti-PD-L1 group). Mice were then analysed at day 14 for LCMV-specific $CD8^+$ T-cell responses, viral titre, and liver immunopathlogy. **b**, Numbers of LCMV-specific (D^bGP33^+ and D^bGP276^+) $CD8^+$ T cells. **c**, Viral titre in the indicated tissues. **d**–**f**, Immunopathological assessment. Serum levels of alanine aminotransferase (ALT) (**d**), liver pathology score (**e**), and number of $TUNEL^+$ sinusoidal cells and hepatocytes (**f**). Results were pooled from 2-4 experiments with n = 2-5 per group in each experiment (**b**–**f**). For serum ALT levels, serum samples were pooled from 2-3 mice. TUNEL staining was done on one of the representative experiments with n = 4 per group. Data are presented as geometric mean and 95% CI (**b**) or mean and SD (**c**–**f**) with p values. Statistical comparisons were performed using two-tailed unpaired Mann-Whitney test (**b**), or two-tailed unpaired t-test (**c**–**f**). ALT, alanine aminotransferase. TUNEL, terminal deoxynucleotidyl transferase dUTP nick end labelling.

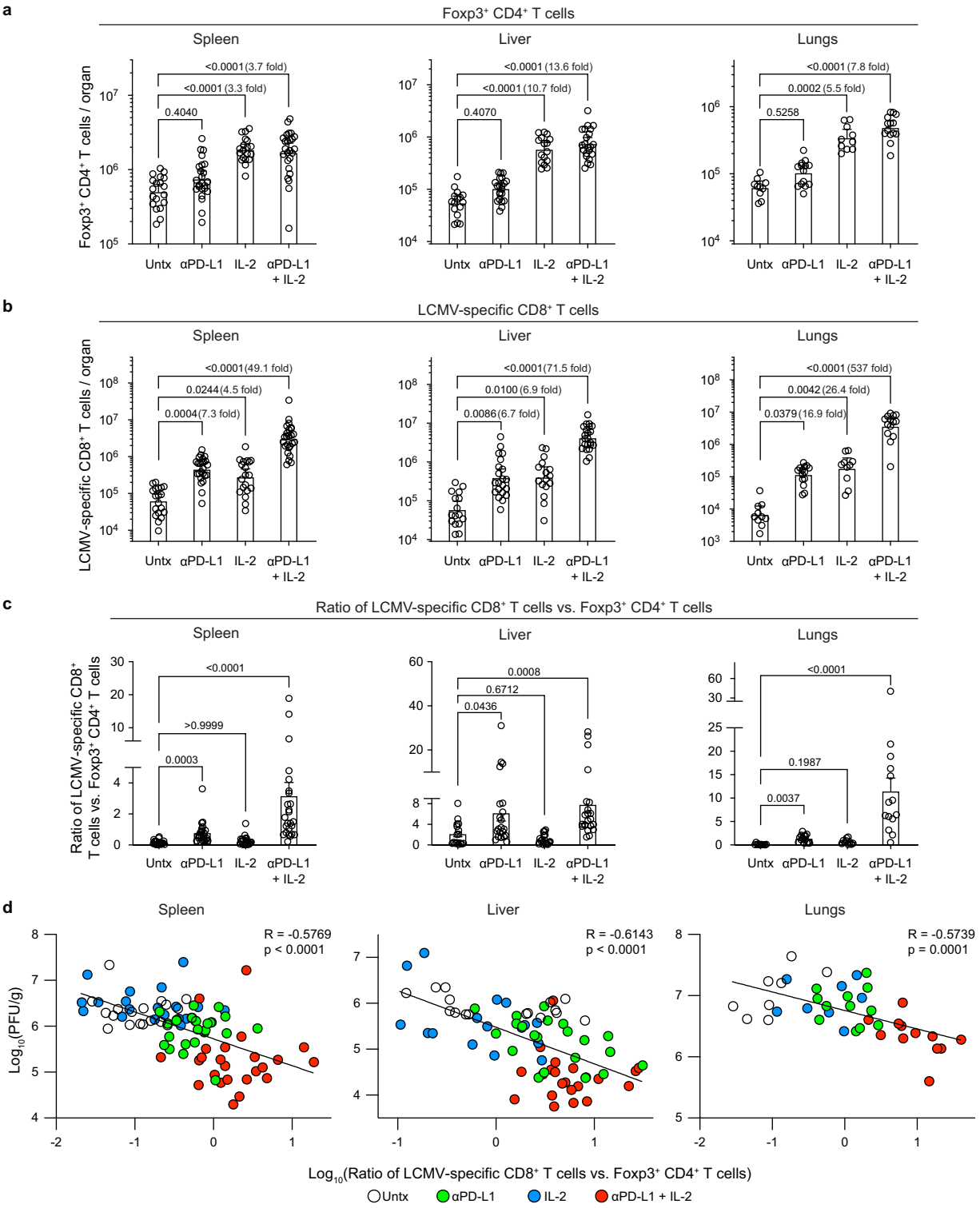

Extended Data Fig. 8 | PD-1 + IL-2 combination therapy results in a more favourable CD8⁺ effector/CD4⁺ Treg ratio compared to IL-2 monotherapy. Mice chronically infected with were either left untreated, or treated with anti-PD-L1 antibody alone, IL-2 therapy alone, or combination therapy. **a**, Numbers of FOXP3⁺ CD4⁺ regulatory T cells (Tregs) in the indicated tissues. **b**, Numbers of LCMV-specific (D^bGP33^+ and D^bGP276^+) CD8⁺ T cells. **c**, Ratio of LCMV-specific (D^bGP33^+ and D^bGP276^+) CD8⁺ T cells vs. FOXP3⁺ CD4⁺ T cells (CD8⁺ effector/CD4⁺ Treg ratio). **d**, Correlation between viral titre and CD8⁺ effector/CD4⁺ Treg ratio in the various tissues. Results were pooled from 5-8 experiments with n = 2-4 per group in each experiment. Data are presented as geometric mean and 95% CI (**a**, **b**), mean and SEM (**c**), or linear regression line and Pearson correlation coefficient (two-tailed) (**d**) with p values. Statistical comparisons were performed using Kruskal-Wallis test with Dunn's multiple-comparison test (**a**–**c**). Untx, untreated.

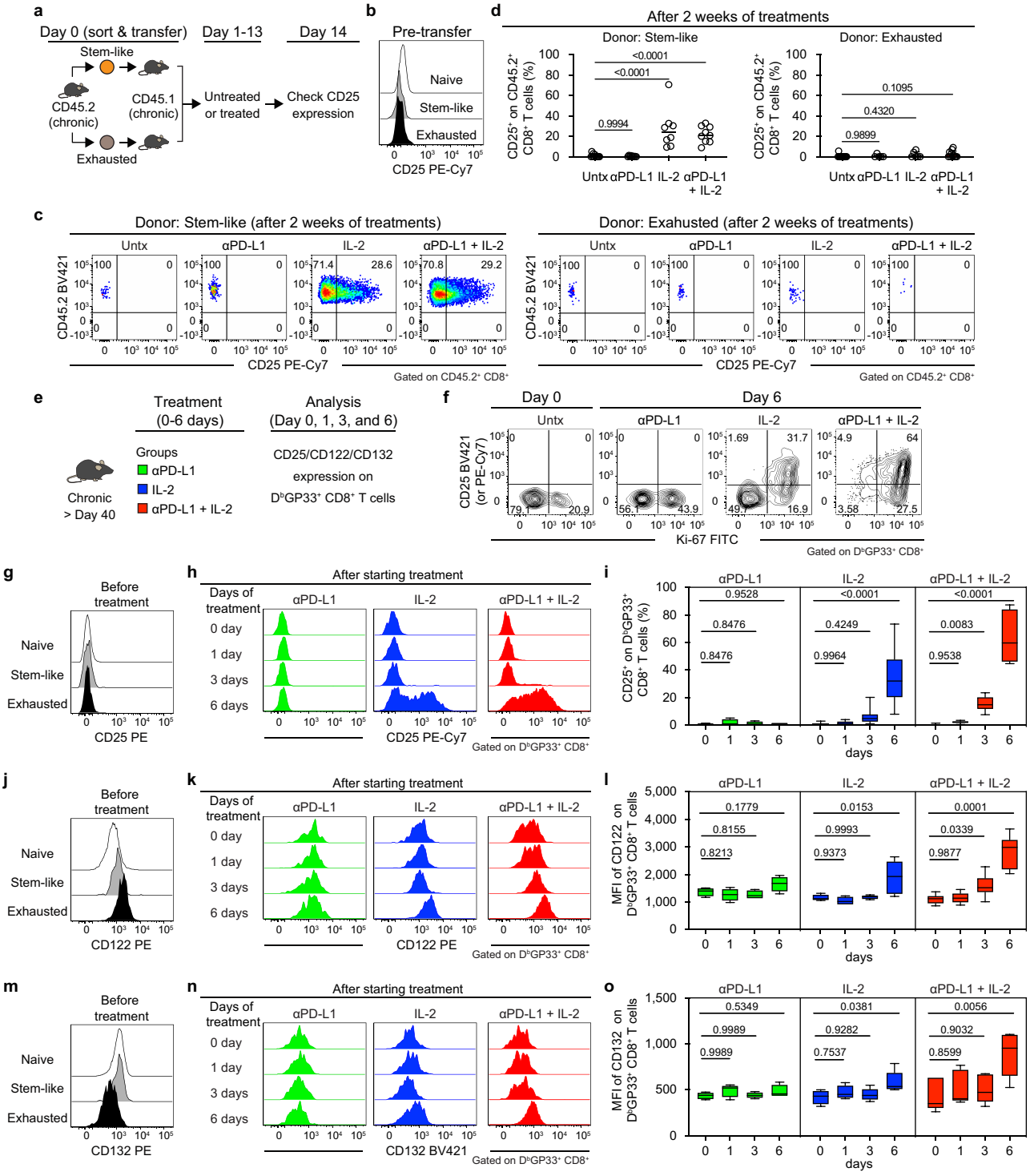

Extended Data Fig. 9 | See next page for caption.

Extended Data Fig. 9 | PD-1$^+$TCF1$^+$ stem-like CD8$^+$ T cells proliferate and differentiate into effector CD8$^+$ T cells expressing the high affinity trimeric (CD25, CD122, CD132) IL-2 receptor after PD-1 + IL-2 combination therapy. **a**, Experimental setup for panels **b**–**d**. Stem-like (PD-1$^+$CXCR5$^+$Tim-3$^-$) and exhausted (PD-1$^+$CXCR5$^-$TIM3$^+$) CD8$^+$ T-cell subsets were sorted from the spleens of LCMV chronically infected CD45.2$^+$ mice and each subset was transferred into infection-matched CD45.1$^+$ recipient mice. Groups of these mice were then either left untreated, given anti-PD-L1 antibody, IL-2 therapy, or combination therapy for 2 weeks. CD25 expression on donor CD45.2$^+$ CD8$^+$ T cells was checked before and after the treatments. **b**, Representative histogram of CD25 expression on the chronic CD8$^+$ T-cell subsets pre-transfer. Naive (CD44^{lo}) CD8$^+$ T cells are also shown as a negative control. **c**, **d**, Representative FACS plots of CD25 expression and summary data of frequency of CD25$^+$ cells in donor CD45.2$^+$ CD8$^+$ T cells originating from stem-like or exhausted CD8$^+$ T cells after the indicated treatments. **e**, Experimental setup for panels **f**–**o**. LCMV chronically infected mice were treated with anti-PD-L1 antibody, IL-2 alone, or combination therapy. Mice were sacrificed on the indicated days and expression of CD25, CD122 and CD132 was examined on LCMV-specific CD8$^+$ T cells in the spleen. **f**, Representative flow plots for the co-expression of CD25 and Ki-67 on D^{b}GP33$^+$ CD8$^+$ T cells at day 0 or day 6 after treatment. **g**, **j**, **m**, Representative histograms showing the expression of CD25 (**g**), CD122 (**j**), and CD132 (**m**) on stem-like and exhausted LCMV-specific DbGP33$^+$ subsets CD8$^+$ T cells before starting the treatment of LCMV chronically infected mice. Naive cells are CD44^{lo} CD8$^+$ T cells present in the same host. **h**, **k**, **n**, Representative histograms showing the expression of CD25 (**h**), CD122 (**k**), and CD132 (**n**) on D^{b}GP33$^+$ CD8$^+$ T cells at days 0-6 after starting the indicated treatment. **i**, **l**, **o**, Summary box plots for the frequency of CD25$^+$ cells (**i**), MFI of CD122 (**l**) and MFI of CD132 (**o**) on D^{b}GP33$^+$ CD8$^+$ T cells after the indicated treatments. Results were pooled from 2-5 experiments with at least 4 mice per group (**a**–**o**). Data are presented as mean and SD (**d**) or the box (25th to 75th percentiles), the whiskers (min to max), and the line (the median) (**i**, **l**, **o**) with p values. Statistical comparisons were performed using one-way ANOVA with Tukey's multiple-comparison test. Untx, untreated.

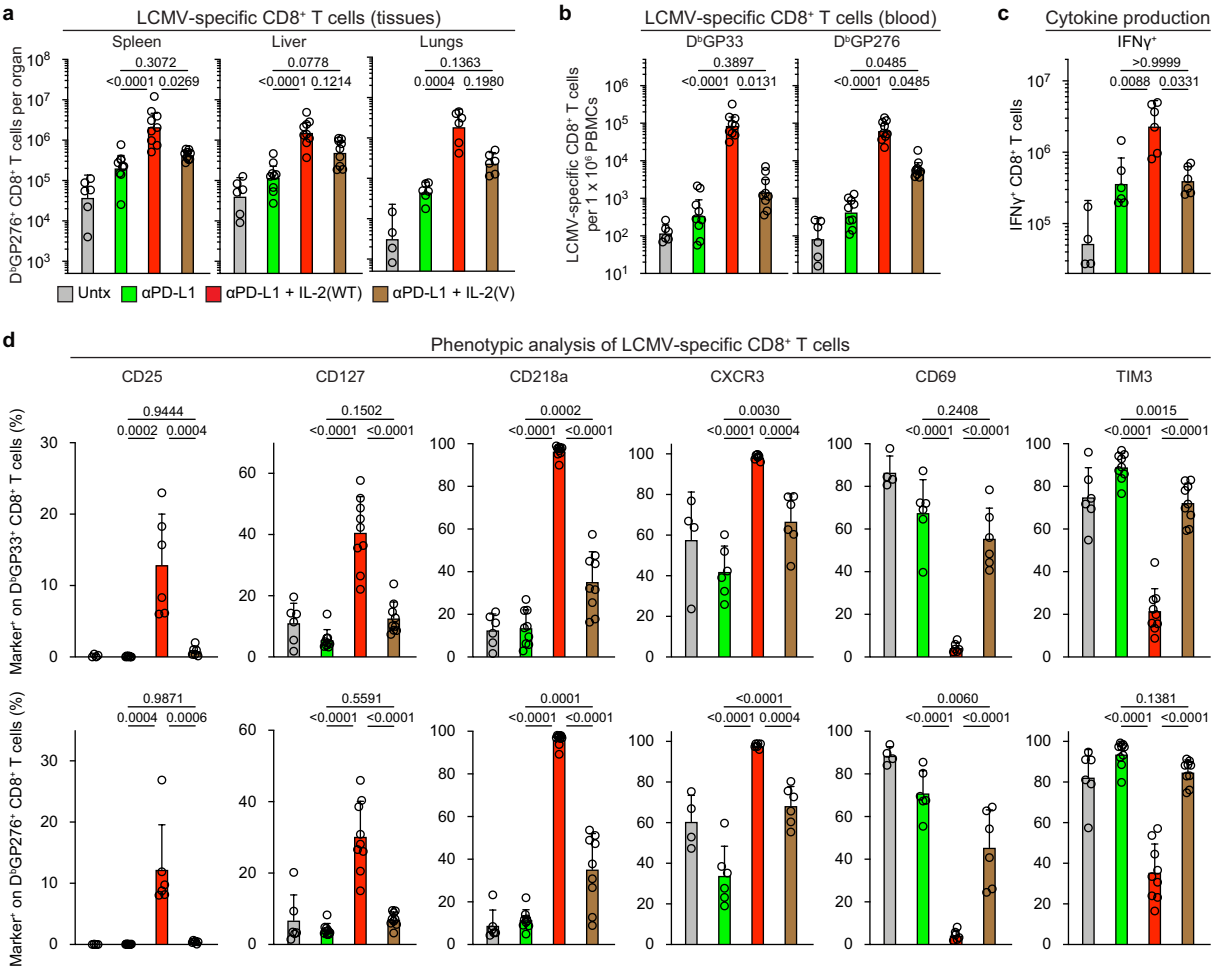

Extended Data Fig. 10 | IL-2(V) does not synergize with PD-1 blockade during chronic LCMV infection. LCMV chronically infected mice were left untreated, or treated with anti-PD-L1 antibody, anti-PD-L1 plus IL-2 wild-type (IL-2(WT)), or anti-PD-L1 plus IL-2(V) (modified IL-2 with abolished CD25 binding) for 2 weeks. **a**, Numbers of D^bGP276^+ $CD8^+$ T cells in the indicated tissues of the four groups of mice. **b**, Numbers of D^bGP33^+ and D^bGP276^+ $CD8^+$ T cells in blood (per 1x 10^6 PBMCs) in the four groups. **c**, Numbers of $IFN\gamma^+$ $CD8^+$ T cells in the different groups. Spleen cells were stimulated with pools of LCMV-specific peptides for 5 h and analysed by intracellular cytokine staining. **d**, Summary data for the expression of various phenotypic markers on D^bGP33^+ and D^bGP276^+ $CD8^+$ T cells after the different treatments. Results were pooled from 2-3 experiments with 2-3 mice per group in each experiment. Data are presented as geometric mean and 95% CI (**a**–**c**) or mean and SD (**d**) with p values. Statistical comparisons were performed using Kruskal-Wallis test with Dunn's multiple-comparison test (**a**–**c**) or one-way ANOVA with Tukey's multiple-comparison test (**d**). Untx, untreated.

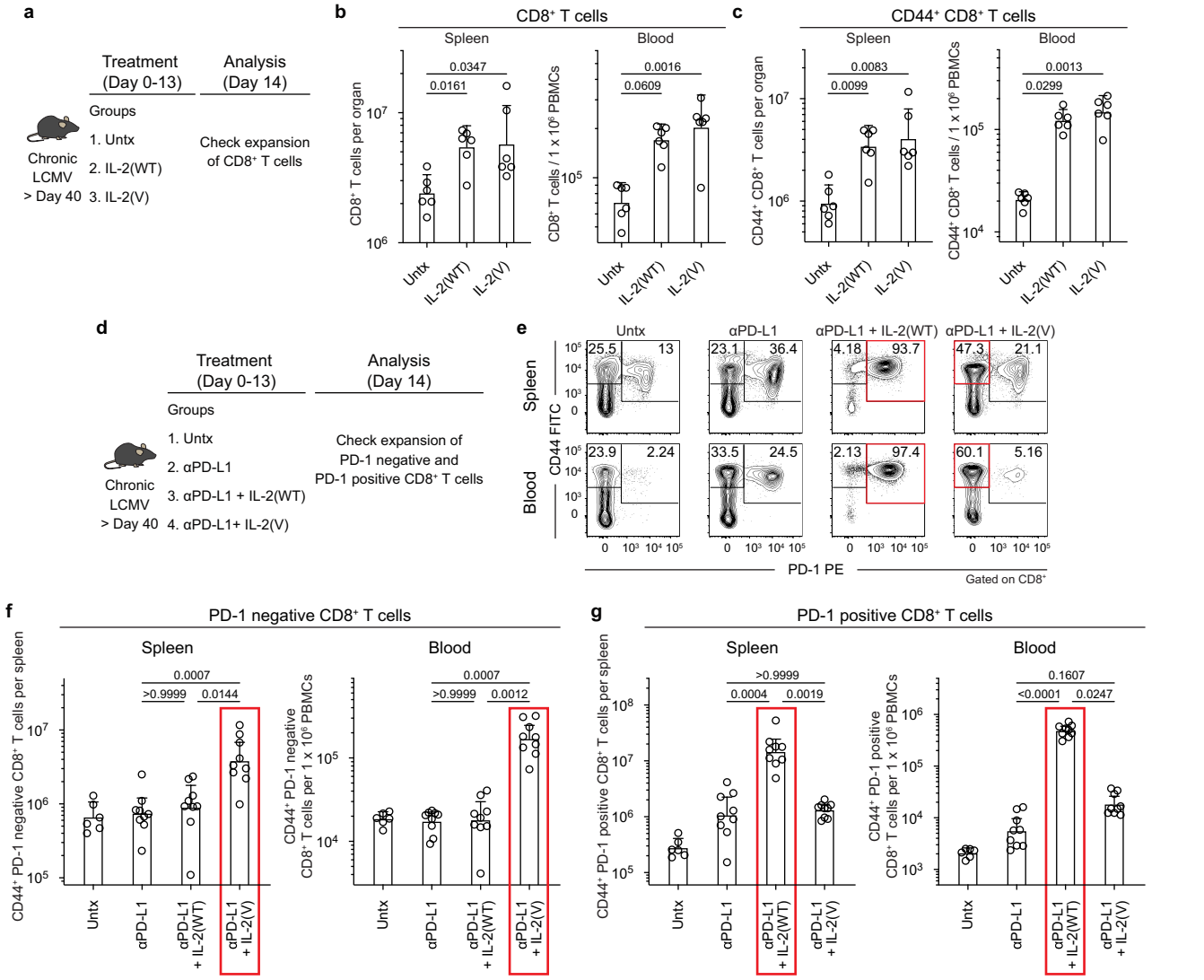

Extended Data Fig. 11 | IL-2(V) is biologically active in vivo but PD-1 + IL-2v combination therapy preferentially expands non-LCMV-specific PD-1 negative CD8⁺ T cells. a, Experimental setup for **b**–**c**. Mice chronically infected with LCMV were left untreated, or treated with IL-2(WT) or IL-2(V) (modified IL-2 with abolished CD25 binding) for 2 weeks. Expansion of CD8⁺ T cells was examined in the spleen and blood in the three groups of mice. **b**, Numbers of CD8⁺ T cells. **c**, Numbers of CD44⁺ CD8⁺ T cells. **d**, Experimental setup for panels **e**–**g**. Chronically infected mice were untreated, or treated with anti-PD-L1 antibody, anti-PD-L1 plus IL-2(WT), or anti-PD-L1 plus IL-2(V) for 2 weeks. Expansion of PD-1 negative and PD-1 positive CD8⁺ T cells was examined in the spleen and blood in the four groups of mice. **e**, Representative FACS plots for CD44 and PD-1 expression on CD8⁺ T cells in the spleen and blood after the various treatments. **f**, Numbers of CD44⁺ PD-1 negative CD8⁺ T cells in the spleen and blood. **g**, Numbers of CD44⁺ PD-1 positive CD8⁺ T cells in the spleen and blood (per 1×10^6 PBMCs) of the four groups. Results were pooled from 3 experiments with at least 6 mice per group. Data are presented as geometric mean and 95% CI (**b**, **c**, **f**, **g**) with p values. Red box highlights preferential expansion of PD-1 negative CD8⁺ T cells by combination therapy with anti-PD-L1 and IL-2(V) whereas combination therapy with anti-PD-L1 and IL-2(WT) expands PD-1 positive CD8⁺ T cells. Statistical comparisons were performed using Kruskal-Wallis test with Dunn's multiple-comparison test. Untx, untreated.

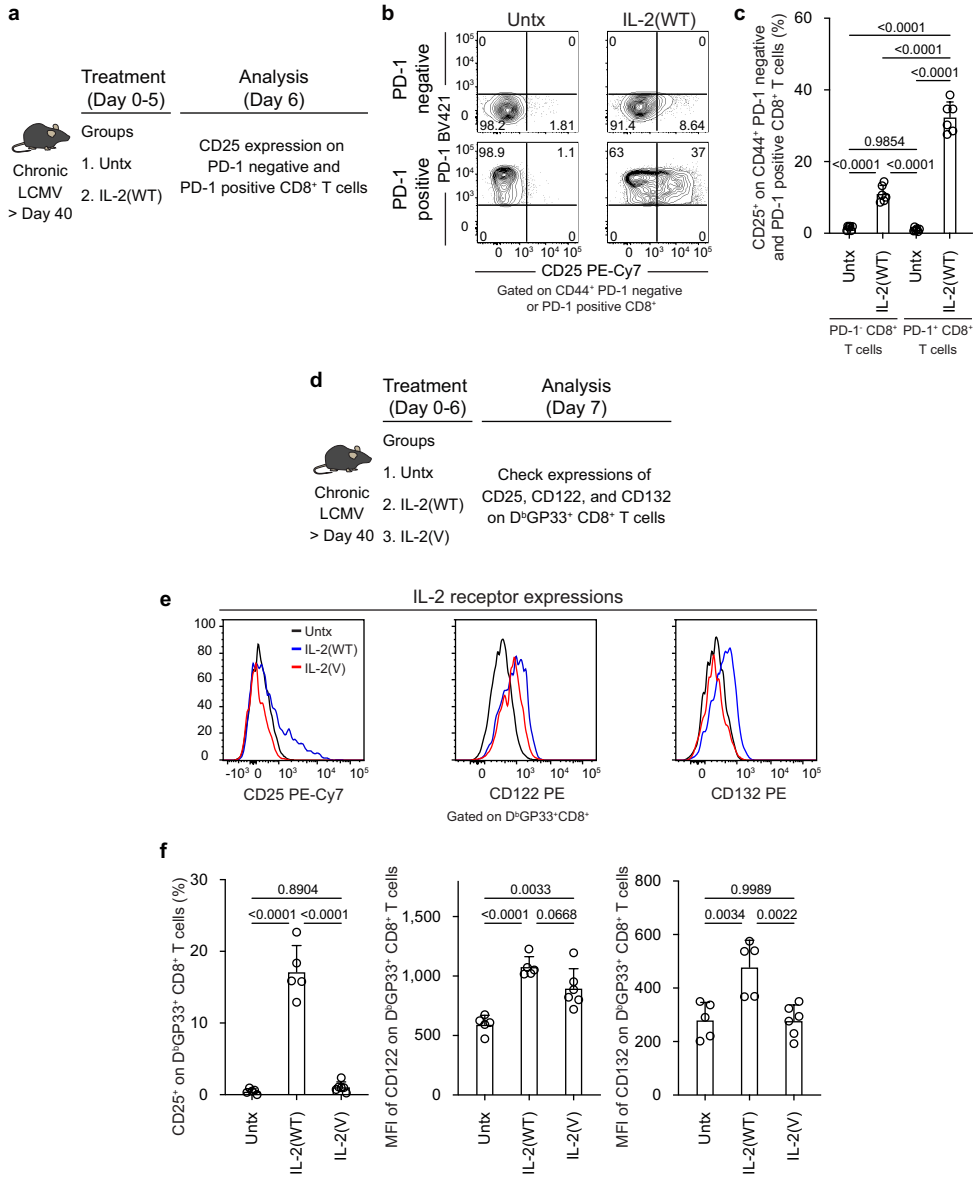

Extended Data Fig. 12 | Effect of IL-2(WT) versus IL-2(V) on LCMV-specific CD8⁺ T cells during chronic infection. a, Experimental design for data in panels **b** and **c**. Mice chronically infected with LCMV (> 40 days post infection) were untreated or treated with IL-2(WT) for 5 days, and CD25 expression was checked on PD-1negative and PD-1⁺ CD8⁺ T cells in the spleen. **b**, Representative FACS plots of CD25 expression. **c**, Summary plots of CD25 expression after IL-2(WT) and IL-2(V) treatments. **d**, Experimental design for data in panels **e** and **f**. Mice chronically infected with LCMV were untreated, treated with IL-2(WT) or treated with IL-2(V) for 6 days. Expression of IL-2 receptors (CD25, CD122, and CD132) on LCMV-specific CD8⁺ T cells in the spleen were examined. **e**, **f**, Representative histograms (**e**) and summary plots (**f**) of expression of IL-2 receptors on D^bGP33^+ CD8⁺ T cells after indicated treatments. Results were pooled from 2 experiments with 2-3 mice per group in each experiment. Data are presented as mean and SD (**c**, **f**) with p values. Statistical comparisons were performed using one-way ANOVA with Tukey's multiple-comparison test. Untx, untreated.

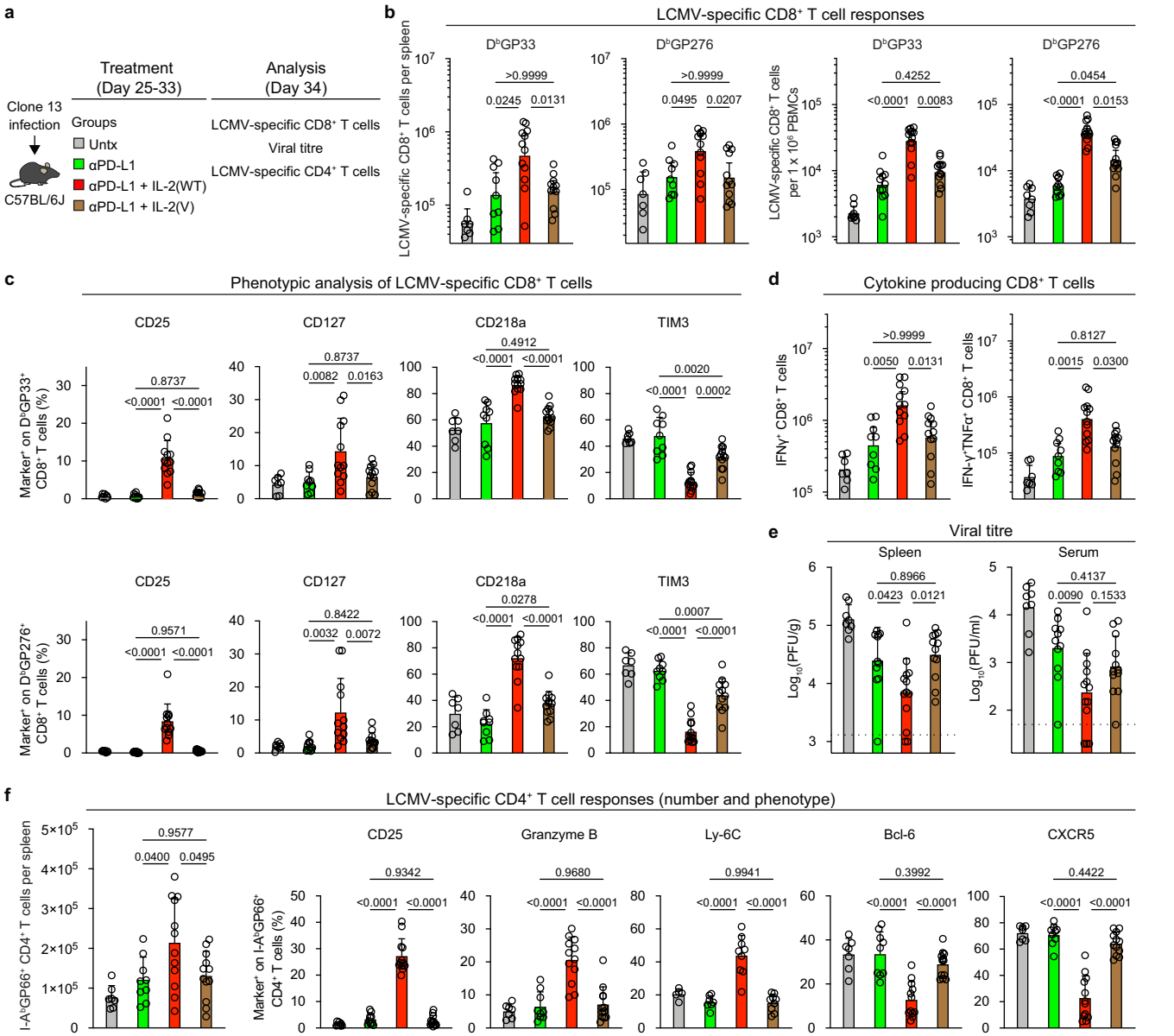

Extended Data Fig. 13 | Comparing the effects of IL-2(WT) cytokine versus IL-2(V) cytokine in PD-1 combination therapy in the LCMV chronic infection model with CD4+ T-cell help. a, Experimental design. Mice infected with LCMV clone 13 (day 25 post-infection) were left untreated, or treated with anti-PD-L1 antibody, anti-PD-L1 plus IL-2(WT), or anti-PD-L1 plus IL-2(V). **b**, Numbers of LCMV-specific D^bGP33^+ $CD8^+$ T cells in the indicated tissues after the various treatments. **c**, Summary data for the expression of phenotypic markers on D^bGP33^+ or D^bGP276^+ $CD8^+$ T cells in the spleen after the different treatments. **d**, Numbers of $IFN\gamma^+$, and $IFN\gamma^+TNF\alpha^+$ LCMV-specific $CD8^+$ T cells in the four groups. Spleen cells were stimulated with pools of LCMV-specific peptides for 5 h and analysed by intracellular staining of cytokines **e**, Viral titre in spleen and serum in the four groups of mice. Dotted line indicates the limit of detection. Results were pooled from 3-4 experiments with 2-5 mice per group in each experiment. Data are presented as geometric mean and 95% CI (**b**, **d**) or mean and SD (**c**, **e**, **f**) with p values. Statistical comparisons were performed using Kruskal-Wallis test with Dunn's multiple-comparison test (**b**, **d**, **f** (number of LCMV-specific $CD4^+$ T cells)) or one-way ANOVA with Tukey's multiple-comparison test (**c**, **e**, **f** (phenotype of LCMV-specific $CD4^+$ T cells)). Untx, untreated.

nature portfolio

Corresponding author(s): Rafi Ahmed

Last updated by author(s): Aug 7, 2022

Reporting Summary

Nature Portfolio wishes to improve the reproducibility of the work that we publish. This form provides structure for consistency and transparency in reporting. For further information on Nature Portfolio policies, see our Editorial Policies and the Editorial Policy Checklist.

Statistics

For all statistical analyses, confirm that the following items are present in the figure legend, table legend, main text, or Methods section.

n/a	Confirmed	
☐	☒	The exact sample size (*n*) for each experimental group/condition, given as a discrete number and unit of measurement
☐	☒	A statement on whether measurements were taken from distinct samples or whether the same sample was measured repeatedly
☐	☒	The statistical test(s) used AND whether they are one- or two-sided *Only common tests should be described solely by name; describe more complex techniques in the Methods section.*
☒	☐	A description of all covariates tested
☐	☒	A description of any assumptions or corrections, such as tests of normality and adjustment for multiple comparisons
☐	☒	A full description of the statistical parameters including central tendency (e.g. means) or other basic estimates (e.g. regression coefficient) AND variation (e.g. standard deviation) or associated estimates of uncertainty (e.g. confidence intervals)
☐	☒	For null hypothesis testing, the test statistic (e.g. *F*, *t*, *r*) with confidence intervals, effect sizes, degrees of freedom and *P* value noted *Give P values as exact values whenever suitable.*
☒	☐	For Bayesian analysis, information on the choice of priors and Markov chain Monte Carlo settings
☒	☐	For hierarchical and complex designs, identification of the appropriate level for tests and full reporting of outcomes
☐	☒	Estimates of effect sizes (e.g. Cohen's *d*, Pearson's *r*), indicating how they were calculated

Our web collection on statistics for biologists contains articles on many of the points above.

Software and code

Policy information about availability of computer code

Data collection	FACS data was collected on BD Canto II, LSR II, or FACSymphony A3 using FACSDiva v8.0.1.
Data analysis	FACS data: Flowjo v.9.9.6 or v10.8.1, GraphPad Prism v.9.3.1 RNA-seq analysis:R Studio v.1.3.1093, HISAT2 v.2.1.0, featureCounts v.1.5.2, DESeq2 v.1.24.0, ggplot2 v.3.3.2, Microsoft Excel 14.7.7 Single Cell RNA-seq:CellRanger v3.1, Seurat v.3.0, VISION R package v.1.1.0. ATAC-seq:bowtie2 v.2.2.4, MACS2 v.2.1.1, IGV v2.11.0 Figure layout: Adobe Illustrator 2021

For manuscripts utilizing custom algorithms or software that are central to the research but not yet described in published literature, software must be made available to editors and reviewers. We strongly encourage code deposition in a community repository (e.g. GitHub). See the Nature Portfolio guidelines for submitting code & software for further information.

Data

Policy information about availability of data

All manuscripts must include a data availability statement. This statement should provide the following information, where applicable:

- Accession codes, unique identifiers, or web links for publicly available datasets
- A description of any restrictions on data availability
- For clinical datasets or third party data, please ensure that the statement adheres to our policy

The data that support the findings of this study are available from the corresponding author upon reasonable request.

Field-specific reporting

Please select the one below that is the best fit for your research. If you are not sure, read the appropriate sections before making your selection.

☒ Life sciences ☐ Behavioural & social sciences ☐ Ecological, evolutionary & environmental sciences

For a reference copy of the document with all sections, see nature.com/documents/nr-reporting-summary-flat.pdf

Life sciences study design

All studies must disclose on these points even when the disclosure is negative.

Sample size	No statistical methods were used to predetermine sample size. Sample sizes were chosen based on previous experiences (West E. E. et al, PD-L1 blockade synergizes with IL-2 therapy in reinvigorating exhausted T cells. J Clin Invest 123, 2604-2615, doi:10.1172/JCI67008 (2013).), balancing statistical robustness and animal welfare.
Data exclusions	Four samples in adoptive transfer expereriments were excluded. Those samples were difficult to analyze due to the high background for the staining.
Replication	All data was reliably reproduced. The number of repeats and sample sizes are provided in each figure legend.
Randomization	LCMV chronically infected mice were randomly assigned to experimental groups.
Blinding	Investigators were not blinded to group allocation during experimental setup, data collection, and analysis. No blinding was performed since we did not have the personnel resources to consistently perform blinding.

Reporting for specific materials, systems and methods

We require information from authors about some types of materials, experimental systems and methods used in many studies. Here, indicate whether each material, system or method listed is relevant to your study. If you are not sure if a list item applies to your research, read the appropriate section before selecting a response.

Materials & experimental systems

n/a	Involved in the study
☐	☒ Antibodies
☐	☒ Eukaryotic cell lines
☒	☐ Palaeontology and archaeology
☐	☒ Animals and other organisms
☒	☐ Human research participants
☒	☐ Clinical data
☒	☐ Dual use research of concern

Methods

n/a	Involved in the study
☒	☐ ChIP-seq
☐	☒ Flow cytometry
☒	☐ MRI-based neuroimaging

Antibodies

Antibodies used

Antibodies used for staining cells in vitro
#Catalogue, Name, Clone, Supplier, Dilution
561522, anti-Bcl-6 PE, K112-91, BD Biosciences, 1:20
741050, anti-CD4 BUV496, RM4-5, BD Biosciences, 1:500
741217, anti-CD4 BUV563, RM4-5, BD Biosciences, 1:500
553046, anti-CD4 FITC, RM4-5, BD Biosciences, 1:500
560782, anti-CD4 V500, RM4-5, BD Biosciences, 1:500
100548, anti-CD4 BV605, RM4-5, Biolegend, 1:500
25-0042-82, anti-CD4 PE-Cy7, RM4-5, Thermo Fisher Scientific, 1:500
47-0042-82, anti-CD4 APC-eFluor 780, RM4-5, Thermo Fisher Scientific, 1:500
563786, anti-CD8a BUV496, 53-6.7, BD Biosciences, 1:100
748535, anti-CD8a BUV563, 53-6.7, BD Biosciences, 1:100
100753, anti-CD8a BV421, 53-6.7, Biolegend, 1:150
563152, anti-CD8a BV605, 53-6.7, BD Biosciences, 1:100
553036, anti-CD8a PerCP, 53-6.7, BD Biosciences, 1:100
553035, anti-CD8a APC, 53-6.7, BD Biosciences, 1:100
740006, anti-CD8b.2 BV421, 53-5.8, BD Biosciences, 1:200
749028, anti-CD19 BUV563, 1D3, BD Biosciences, 1:150
115546, anti-CD19 BV510, 1D3, Biolegend, 1:150
115540, anti-CD19 BV605, 1D3, Biolegend, 1:150
25-0193-82, anti-CD19 PE-Cy7, 1D3, Thermo Fisher Scientific, 1:150

47-0193-82, anti-CD19 APC-eFluor 780, 1D3, Thermo Fisher Scientific, 1:150
102043, anti-CD25 BV421, PC61, Biolegend, 1:100
102008, anti-CD25 PE, PC61, Biolegend, 1:100
566498, anti-CD25 BB700, PC61, BD Biosciences, 1:100
25-0251-82, anti-CD25 PE-Cy7, PC61.5, Thermo Fisher Scientific, 1:100
122010, anti-CD28 PE, E18, Biolegend, 1:100
48-0291-82, anti-CD29 eFluor 450, HMb1-1, Thermo Fisher Scientific, 1:100
741921, anti-CD44 BUV805, IM7, BD Biosciences, 1:500
561859, anti-CD44 FITC, IM7, BD Biosciences, 1:500
56-0441-82, anti-CD44 Alexa Fluor 700, IM7, Thermo Fisher Scientific, 1:100
109832, anti-CD45.2 BV421, 104, Biolegend, 1:100
109814, anti-CD45.2 APC, 104, Biolegend, 1:100
103608, anti-CD49d PE, R1-2, Biolegend, 1:100
564108, anti-CD62L BV650, MEL-14, BD Biosciences, 1:100
25-0691-82, anti-CD69 PE-Cy7, H1.2F3, Thermo Fisher Scientific, 1:100
127215, anti-CD73 BV605, TY/11.8, Biolegend, 1:100
25-1011-82, anti-CD101 PE-Cy7, Moushi101, Thermo Fisher Scientific, 1:100
17-1081-82, anti-CD101 APC, Moushi101, Thermo Fisher Scientific, 1:100
53-1071-82, anti-CD107a Alexa Fluor 488, 1D4B, Thermo Fisher Scientific, 1:200
740032, anti-CD119 BV421, GR20, BD Biosciences, 1:100
123210, anti-CD122 PE, TM-β1, Biolegend, 1:100
12-1271-83, anti-CD127 PE, A7R34, Thermo Fisher Scientific, 1:100
740039, anti-CD132 BV421, TUGm2, BD Biosciences, 1:100
132306, anti-CD132 PE, TUGm2, Biolegend, 1:100
740096, anti-CD160 BV421, CNX46-3, BD Biosciences, 1:100
12-5183-82, anti-CD218a PE, P3TUNYA, Thermo Fisher Scientific, 1:100
46-5183-82, anti-CD218a PerCP-eFluor 710, P3TUNYA, Thermo Fisher Scientific, 1:100
25-5183-82, anti-CD218a PE-Cy7, P3TUNYA, Thermo Fisher Scientific, 1:100
125221, anti-CD223 BV421, C9B7W, Biolegend, 1:100
128812, anti-CD226 PE-Cy7, 10E5, Biolegend, 1:100
746651, anti-CXCR3 BV480, CXCR3-173, BD Biosciences, 1:100
25-1831-82, anti-CXCR3 PE-Cy7, CXCR3-173, Thermo Fisher Scientific, 1:100
145512, anti-CXCR5 BV421, L138D7, Biolegend, 1:50
145522, anti-CXCR5 PE-Dazzle, L138D7, Biolegend, 1:50
149031, anti-CX3CR1 BV785, SA011F11, Biolegend, 1:500
149006, anti-CX3CR1 PE, SA011F11, Biolegend, 1:500
134804, anti-BTLA PE, 8F4 , Biolegend, 1:100
25-4875-82, anti-Eomes PE-Cy7, Dan11mag, Thermo Fisher Scientific, 1:100
25-5773-82, anti-Foxp3 PE-Cy7, FJK-16s , Thermo Fisher Scientific, 1:250
12-5831-82, anti-granzyme A PE, GzA-3G8.5, Thermo Fisher Scientific, 1:100
396414, anti-granzyme B BV421, QA18A28, Biolegend, 1:20
GRB04, anti-granzyme B PE, GB11, Thermo Fisher Scientific, 1:20
107706, anti-ICOS PE, 15F9, Biolegend, 1:100
554428, anti-IL-2 PE, JES6-5H4, BD Biosciences, 1:100
505830, anti-IFN-γ BV421, XMG1.2, Biolegend, 1:100
566097, anti-IFN-γ BV480, XMG1.2, BD Biosciences, 1:100
564336, anti-IFN-γ BV711, XMG1.2, BD Biosciences, 1:100
554413, anti-IFN-γ APC, XMG1.2, BD Biosciences, 1:100
556026, anti-Ki-67 FITC, B56, BD Biosciences, 1:20
128032, anti-Ly-6C BV421, HK1.4, Biolegend, 1:500
566987, anti-Ly-6C R718, AL-21, BD Biosciences, 1:500
135218, anti-PD-1 BV421, 29F.1A12, Biolegend, 1:100
135220, anti-PD-1 BV605, 29F.1A12, Biolegend, 1:100
135231, anti-PD-1 BV711, 29F.1A12, Biolegend, 1:100
109104, anti-PD-1 PE, RMP1-30, Biolegend, 1:100
109112, anti-PD-1 APC, RMP1-30, Biolegend, 1:100
741893, anti-Slamf6 BUV737, 13G3, BD Biosciences, 1:100
6444, anti-TCF-1 Alexa Fluor 488, C63D9, Cell Signaling Technology, 1:50
564217, anti-TCF-1 PE, S33-966, BD Biosciences, 1:100
747620, anti-Tim-3 BUV395, 5D12, BD Biosciences, 1:100
FAB1529G, anti-Tim-3 Alexa Fluor 488, 215008, R&D systems, 1:20
FAB1529P, anti-Tim-3 PE, 215008, R&D systems1:20
12-5825-82, anti-T-bet PE, eBio4B10 (4B10), Thermo Fisher Scientific, 1:100
554418, anti-TNF FITC, MP6-XT22, BD Biosciences, 1:100
554419, anti-TNF PE, MP6-XT22, BD Biosciences, 1:100
12-6502-82, anti-Tox PE, TXRX10, Thermo Fisher Scientific, 1:100
130-090-855, Anti-APC MicroBeads, Miltenyi Biotec
130-104-075, CD8a+ T Cell Isolation Kit, mouse, Miltenyi Biotec

Antibodies used for in vivo injection
#Catalogue, Name, Clone, Supplier, Amount
NA, rat anti-mouse PD-L1, 10F.9G2, Prepared in house, 200 µg/mouse/injection
BE0090, rat IgG2b isotype control, LTF-2, BioXCell, 200 µg/mouse/injection
NA, anti-mouse PD-L1 with DAPG mutation, NA, Roche, 200 µg/mouse/injection
BE0083, mouse IgG1 isotype control, MOPC-21, BioXCell, 200 µg/mouse/injection
BE0003-1, anti-mouse CD4, GK1.5, BioXCell, 300 µg/mouse/injection

NA, rat-mouse chimeric anti-mouse CD25, PC61-mIgG1 (N297Q), Biogen, 200 µg/mouse/injection
BE0061, anti-mouse CD8a2.43, BioXCell, 200 µg/mouse/injection

Validation

All the commercial antibodies are validated by the manufacturers and previous studies of others.
Detailed information and references are shown in https://www.bdbiosciences.com, https://www.biolgend.com, https://www.thermofisher.com, https://www.cellsignal.com, http://www.rndsystems.com, and https://bxcell.com, and https://www.miltenyibiotec.com.

Rat anti-mouse PD-L1 antibody (10F.9G2) was validated by our previous study (Barber, D. L. et al. Restoring function in exhausted CD8 T cells during chronic viral infection. Nature 439, 682-687, doi:10.1038/nature04444 (2006)).

Anti-mouse PD-L1 antibody with DAPG mutation was validated by Roche and the previous study (Klein, C. et al. Cergutuzumab amunaleukin (CEA-IL2v), a CEA-targeted IL- 2 variant-based immunocytokine for combination cancer immunotherapy: Overcoming limitations of aldesleukin and conventional IL-2-based immunocytokines. Oncoimmunology 6, e1277306, doi:10.1080/2162402X.2016.1277306 (2017)).

Rat-mouse chimeric anti-mouse CD25 was validated by Biogen and the previous study (Huss, D. J. et al. Anti-CD25 monoclonal antibody Fc variants differentially impact regulatory T cells and immune homeostasis. Immunology 148, 276-286, doi:10.1111/imm.12609 (2016)).

Eukaryotic cell lines

Policy information about cell lines

Cell line source(s)	Vero E6 cells (ATCC)
Authentication	Vero E6 cells were not authenticated.
Mycoplasma contamination	Cell lines were not tested for mycoplasma contamination.
Commonly misidentified lines (See ICLAC register)	No commonly misidentified lines were used in this study.

Animals and other organisms

Policy information about studies involving animals; ARRIVE guidelines recommended for reporting animal research

Laboratory animals	Six- to 8-week-old female C57BL/6J and B6.SJL-Ptprca Pepcb/BoyJ mice were purchased from the Jackson Laboratory. All animal 848 experiments were performed in accordance with National Institutes of Health and the Emory University Institutional Animal Care and Use Committee guidelines. The following housing conditions for the mice are used. -Light Cycle is 7:00 am ON, 7:00 pm OFF -Temperature is between 68-74 degrees Fahrenheit -Humidity is between 30-70 g/m3
Wild animals	No wild animals were used.
Field-collected samples	No samples were collected from the field.
Ethics oversight	All animal experiments were performed in accordance with National Institutes of Health and the Emory University Institutional Animal Care and Use Committee guidelines.

Note that full information on the approval of the study protocol must also be provided in the manuscript.

Flow Cytometry

Plots

Confirm that:

☒ The axis labels state the marker and fluorochrome used (e.g. CD4-FITC).

☒ The axis scales are clearly visible. Include numbers along axes only for bottom left plot of group (a 'group' is an analysis of identical markers).

☒ All plots are contour plots with outliers or pseudocolor plots.

☒ A numerical value for number of cells or percentage (with statistics) is provided.

Methodology

Sample preparation	Lymphocyte isolation Lymphocytes were isolated from the blood, spleen, liver, and lung as described previously. Briefly, spleens were dissociated by passing them through a 70 µm cell strainer (Corning). Livers were perfused with pre-cold PBS and homogenized via

mechanical disruption. Lungs were treated with 1.3 mM EDTA in HBSS for 30 min at 37 °C, shaking at 200 rpm, followed by treatment with 150 U/ml collagenase (Thermo Fisher Scientific) in RPMI 1640 medium containing 5 % FBS, 1 mM MgCl2, and 1mM CaCl2 for 60 min at 37 °C shaking at 200 rpm. Collagenase treated lung tissues were homogenized and filtered through a 70 µm cell strainer. Lymphocytes from livers and lungs were purified by a 44–67% Percoll gradient (800 g at 20 °C for 20 min).

Flow cytometry and in vitro stimulations
For cell surface staining, antibodies were added to cells at dilutions of 1:50-1:500 in PBS supplemented with 2% FBS and 0.1% sodium azide for 30 min on ice. Cells were washed 3 times, fixed with Fixation/Permeabilization solution (BD Biosciences). For detecting cytokine production, 1 x 106 spleen cells were stimulated with pool of 9 LCMV-specific peptides (GP33-41, GP70-77, GP92-101, GP118-125, GP276-286, NP166-175, NP205-212, NP235-249, and NP396-404; 200 ng/ml each) in a 96-well round bottom plate for 5 hours at 37 C in a CO2 incubator in the presence of GolgiPlug (BD Biosciences). To detect degranulation, splenocytes were stimulated with pool of 9 LCMV-specific peptides for 5 h in the presence of GolgiPlug, GolgiStop (BD Biosciences), and anti-CD107a Alexa Fluor 488 (dilution, 1:200) (Thermo Fisher Scientific). For examining the responsiveness of LCMV-specific CD8+ T cells to inflammatory cytokines, 1 x 106 splenocytes were cultured with recombinant mouse IL-12 and IL-18 (Both were from R&D systems, 20 ng/ml each) for 5 hours, and GolgiPlug was added, followed by culturing for 1 hour. Intracellular staining was performed by using BD Cytofix/Cytoperm protocol. For detecting intranuclear proteins, Foxp3 staining buffer set (Thermo Fisher Scientific) was used according to manufacturer's instructions. To detect LCMV-specific CD4+ T cells, splenocytes were stained with I-AbGP66-77 tetramer (DIYKGVYQFKSV; NIH Tetramer Core Facility, Emory University) at 37°C for 2 h (dilution, 1:200), followed by cell surface staining as described. Samples were acquired on Canto II, LSR II, or FACSymphony A3 (BD Biosciences), and data were analyzed by using FlowJo (ver. 9.9.6 or 10.8.1, BD Biosciences).

Cell sorting
Cell sorting was performed by FACS Aria II (BD Biosciences). For RNA-seq, scRNA-seq (10X Genomics), and ATAC-seq analysis, LCMV chronically infected mice (> day 40 p.i.) were untreated or treated with various therapeutic modalities for 2 weeks, and DbGP33+ CD8+ T cells in spleens were sorted from pooled spleens (n=1-18). Before the sort, DbGP33+ CD8+ T cells were enriched by staining DbGP33-APC tetramer, labeling them with anti-APC MicroBeads (Miltenyi Biotec), followed by magnetic separation with LS column (Miltenyi Biotec). Naïve (CD44lo) CD8+ T cells were sorted from pooled spleens from uninfected mice (n=2). For chemotaxis assay, splenocytes were isolated from LCMV chronically infected mice left untreated or treated with different treatment regimens (n=1-8), CD8+ T cells were enriched by using CD8+ T cell isolation kit (Miltenyi Biotec), followed by magnetic separation with LS column (Miltenyi Biotec), and PD-1+ CD8+ T cells were sorted. For experiments of adoptive transfer of two CD8a+ T-cell subsets, splenocytes were isolated from LCMV chronically infected mice (n=20-53), and 5 x 104 to 1 x 105 of two (PD-1+CXCR5+Tim-3- and PD-1+CXCR5-Tim-3+) CD8+ T-cell subsets were sorted. The purities of the sorted cells were more than 95%.

Analysis of multiparameter conventional flow cytometry
For examining phenotypes of LCMV-specific CD8+ T cells, conventional 19-color flow cytometry data of DbGP33+ CD8+ T cells after different treatments were concatenated, and subjected to UMAP plugins (nearest neighbors = 15, minimum distance = -0.5, and number of components = 2) and FlowSOM clustering algorithm (number of meta clusters = 3) using parameters of TCF-1 Alexa Fluor 488, granzyme B BV421, Tim-3 BUV395, CX3CR1 BV785, CD101 PE-Cy7, CD218a PE, CXCR5 PE-Dazzle, Slamf6 BUV737, CD73 BV605, CXCR3 BV480, Ly-6C R700, and CD44 BUV805 in FlowJo ver. 10.8.1 (BD Biosciences).
To determine which CD8+ T cells in 3 clusters produced effector cytokines or degranulated after stimulation with LCMV-specific peptides, 14-color flow cytometry data of PD-1+ CD8+ T cells were concatenated and used for the subsequent analysis as described above using parameters of TCF-1 Alexa Fluor 488 (or PE), granzyme B BV421, CX3CR1 BV785, CD101 APC, CD218a PerCP-eFluor710 (or PE), Tim-3 BUV395, Slamf6 BUV737, and CD44 BUV805. Distribution of IFN-γ+, IFN-γ+TNF-α+. IFN-γ+IL-2+, and IFN-γ+CD107a+ cells were checked in the defined 3 clusters. TCF-1 was excluded from the staining panel when intracellular IL-2 staining was performed by BD Cytofix/Cytoperm protocol due to the incompatibility of PE anti-IL-2 (clone JES6-SH4, BD Biosciences) for Foxp3 staining buffer protocol.
For testing which CD8+ T cells in 3 clusters produced IFN-γ in response to IL-12 + IL-18 stimulation, DbGP33+ CD8+ T cells from mice treated with various regimens were concatenated and subjected to the subsequent analysis as described above by using parameters of TCF-1 Alexa Fluor 488, granzyme B BV421, CX3CR1 BV785, CD101 PE-Cy7, CD218a PE, Tim-3 BUV395, Slamf6 BUV737, and CD44 BUV805. IFN-γ+ cells were identified in the defined 3 clusters.

Instrument

Cell sorting was performed by FACS Aria II (BD Biosciences).
FACS data was collected on BD Canto II, LSR II, or FACSymphony A3 using FACSDiva v8.0.1.

Software

FACS data were analyzed by using FlowJo (ver. 9.9.6 or 10.8.1, BD Biosciences) with UMAP and FlowSOM plugins.

Cell population abundance

The purities of the sorted cells were more than 95%.

Gating strategy

Refer to Extended Data Fig. 2a for gating strategy for sorting two PD-1+ CD8+ T-cell subsets from LCMV chronically infected mice for adoptive transfer experiments.

All other gating strategies for the experiments are provided as Supplementary Information.

☒ Tick this box to confirm that a figure exemplifying the gating strategy is provided in the Supplementary Information.